Modelling principal stress orientations in the Arabian Plate using plate velocities



Santiago Peña Clavijo^{1,2*}, Anindita Dash³, Guillaume Baby², Abdulkader M. Alafifi² and Thomas Finkbeiner²

¹Applied Geosciences, TNO innovation for life, Utrecht 3584 CB, The Netherlands

D SPC, 0000-0002-8203-2027

*Correspondence: sapenacl91@gmail.com

Abstract: We model maximum principal horizontal stress orientations in the Arabian Plate using a 3D finite element approach in conjunction with plate velocities. To capture the impact of geometry and tectonics, the model considers an accurate plate boundary shape and associated deformations. Three primary geological units represent plate architecture: sedimentary cover, crust and upper mantle. The mesh resolution varies to capture important geometrical features. Subsequently, we calculate the stress field using the force balance equation. Displacement boundary conditions are evaluated as accumulative deformation.

NE–SW maximum principal horizontal stress (S_{Hmax}) azimuths dominate in northeastern Saudi Arabia and Kuwait, whilst NW–SE to NNW–SSE define the Dead Sea area. The Red Sea Basin and Saudi Arabia's interior is characterized by north–south S_{Hmax} azimuths. Iraq's western area shows azimuths from NNW–SSE to NW–SE due to the collision at the Zagros Mountain Range, but changes to NE–SW in the east at the Zagros fold-and-thrust belt.

An extensive literature review reveals publicly available S_{Hmax} azimuth data which augment the sparse records compiled in the World Stress Map database. Our simulated S_{Hmax} azimuths are consistent with these data. The results further corroborate ongoing tectonic processes, deepen our understanding of *in situ* stress variation drivers and inform current elastic deformation mechanisms in the Arabian Plate.

The understating of the present-day in situ stress field in the Earth's crust and its variability is critical for earth science disciplines that require an understanding of geodynamic processes (e.g. Townend and Zoback 2004; Heidbach and Ben-Avraham 2007; Gaucher et al. 2015). In addition, it is important for a range of practical engineering applications, including the production of hydrocarbons and geothermal energy, mine safety, seismic hazard assessment, and underground storage of CO2 (e.g. Cornet et al. 1997; Fuchs and Müller 2001; Heidbach et al. 2019; Zoback 2010; Moeck et al. 2011; Altmann et al. 2014; Ziegler et al. 2016). The importance of mapping the maximum principal horizontal stress (S_{Hmax}) has been demonstrated by the World Stress Map (WSM) Project (Heidbach et al. 2018), which shows that lithospheric in situ stress is controlled by the forces exerted at tectonic plate boundaries, drag forces from slow mantle convection acting at the base of plates and gravity-induced deformation. Following on from this work, we focus this study on the Arabian Plate and similarly model the azimuth of S_{Hmax} . This is particularly pertinent given the region's numerous prolific hydrocarbon resources, associated subsurface developments and engineering projects. Presently, assessing stress magnitudes within the plate remains challenging due to the inaccessibility of most of the existing downhole data and a relative seismic quiescence in the plate's interior (discussed in the section 'The present-day stress pattern in the Arabian Plate: compilation of published data to augment the WSM database'.).

The Arabian Peninsula is part of a small tectonic plate that is characterized by active deformations along its boundaries with: (1) extension and plate divergence in the Red Sea and Gulf of Aden oceans; (2) strike–slip transform along the Dead Sea and Owen Faults; and (3) compression due to plate collision along the Zagros fold belt range (Fig. 1). These tectonic processes acting at the plate boundaries are accompanied by appreciable seismic activity. Furthermore, recent studies have highlighted the occurrence of small earthquakes within the plate

From: Goteti, R., Finkbeiner, T., Ziegler, M. O. and Massiot, C. (eds) *Characterization, Prediction and Modelling of Crustal Present-Day In-Situ Stresses*. Geological Society, London, Special Publications, **546**, https://doi.org/10.1144/SP546-2022-327

© 2024 The Author(s). This is an Open Access article distributed under the terms of the Creative Commons Attribution License (http://creativecommons.org/licenses/by/4.0/). Published by The Geological Society of London. Publishing disclaimer: www.geolsoc.org.uk/pub_ethics

²Ali I. Al-Naimi Petroleum Engineering Research Center, King Abdullah University of Science and Technology, Thuwal 23955, Kingdom of Saudi Arabia

³Rice University, Department of Earth, Environmental and Planetary Sciences, 77005, Houston, Texas, USA

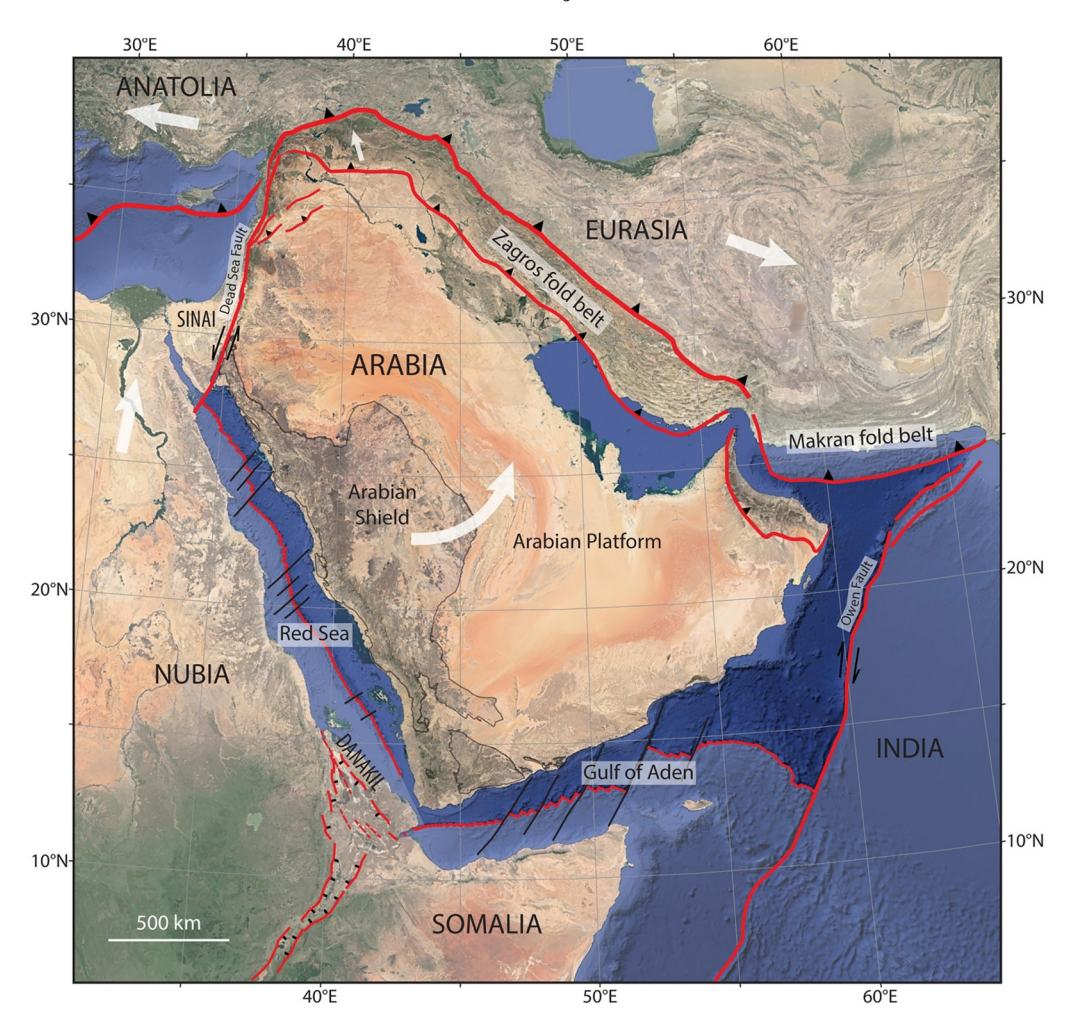


Fig. 1. Regional tectonic map of the Arabian Plate. The plate shares its boundaries with the Nubian Plate (west–SW), the Eurasian Plate (NE), the Indian Plate (east), the Somalian Plate (south), the Anatolian Plate (north), the Sinai Plate (NW) and the Danakil Microplate (SW). Thick arrows show the current relative movement of the plates. Thin arrows show the motion of the plate along the Red Sea and the Gulf of Suez (from Viltres *et al.* 2022). Source: Adapted from Stern and Johnson (2010); Viltres *et al.* (2022); satellite image from Google Earth.

(Al-Shijbi *et al.* 2019). However, the interior of the Arabian Plate is largely aseismic, suggesting rigid plate motion at lithospheric stress levels which are not sufficient to activate pre-existing faults in the interior of the plate (Viltres *et al.* 2022). Thus, analysis and inversion of seismic focal mechanisms for present-day *in situ* stress is not possible. The eastern region of the plate is characterized by substantial horizontal compression, as evidenced by some S_{Hmax} *in situ* stress indicators estimated in boreholes (Ahmed *et al.* 2007, 2014; Ameen *et al.* 2010; Ameen 2014), which impact wellbore integrity, hydrocarbon production and well-stimulation processes. Unfortunately, the WSM database does not

contain any present-day stress indicators (Rajabi *et al.* 2014), even though thousands of oil and gas wells have been drilled in eastern Saudi Arabia, Iraq, Kuwait, SW Iran, Abu Dhabi and Oman.

We use numerical simulations to deepen our understanding of the present-day *in situ* stress state in the Arabian Plate. Specifically, we predict S_{Hmax} azimuths for the whole plate using numerical finite element modelling tools together with a plate velocity model. A simplified, yet accurate, mesh adequately discretizes the brittle lithosphere. The model contains the peninsula's tectonically active boundaries, gravity-induced stresses, other prominent structural elements, and enough lithological

layers to capture mechanical stratigraphies such as the sedimentary cover, the crystalline basement and the upper mantle. We use a 3D unstructured mesh (with finer resolution at critical locations) and solve the linear momentum equation. Boundary conditions are imposed based on the GPS velocity model proposed by Viltres *et al.* (2022). To model the initial stress state, we follow a two-step approach by first applying gravity followed by lateral displacement, as explained in detail in Hergert *et al.* (2015).

For simplicity, we provide simulation results at 4 km depth, which enable us to capture the sedimentary layers in the eastern part of the plate where most of the petroleum activities occur. Thus, we provide a possibility to verify our model against any proprietary data which may later become available in the public domain. However, comparing the S_{Hmax} azimuths recorded in the WSM database (Heidbach *et al.* 2018), and also listed in a few publications (as discussed in the section 'Numerical model'), our simulation results agree well with the available data.

Arabian Plate geology and tectonic stress regime

The Arabian Plate originated around 30 Ma ago during the late Oligocene by rifting the NE African Plate to form the Red Sea and the Gulf of Aden oceans (e.g. Bosworth *et al.* 2005). The NE drift of the plate is accommodated in the north and east by the Zagros and Makran fold-and-thrust belts (Fig. 1). Laterally, the plate is flanked by two major transform fault zones: the left-lateral Dead Sea Fault to the west and the right-lateral Owen Fault to the east (De Lamotte and Leturmy 2014). GPS measurements show that the Arabian Plate is slowly moving north relative to Africa, with spreading rates of 16–22 mm yr⁻¹ in the Gulf of Aden and decreasing northward from 18 to 8 mm yr⁻¹ in the Red Sea (Viltres *et al.* 2022)

The Arabian Plate is a structurally and compositionally complex plate, measuring c. 2600 km north south and c. 3000 km east-west, and tilted toward the east. The Arabian Shield on the western side is composed of Neoproterozoic basement rocks (1000-540 Ma old) formed by amalgamated magmatic arcs overlain by sedimentary and volcanic basins and intruded by granitoids. Locally, Archean and Paleoproterozoic rocks are structurally intercalated in the Neoproterozoic in the southern and eastern parts of the shield (Johnson and Woldehaimanot 2003). The Arabian Platform on the eastern side predominantly accumulated siliciclastic sediments during the Paleozoic and then transitioned to largely marine carbonates during the Mesozoic and Paleogene. The maximum thickness of this sedimentary basin reaches 10 km (e.g. Murris 1980; Geert et al. 2001; Konert et al. 2001; Ziegler 2001). The onset

of the collision between the Arabian and Eurasian Plates at the end of the Oligocene allowed the return of clastic sedimentation at the front of the future Zagros Mountain Range (e.g. Mouthereau 2011), and also in the young rift basins of the Red Sea and the Gulf of Aden (e.g. Leroy *et al.* 2012).

The present-day stress pattern in the Arabian Plate: compilation of published data to augment the WSM database

Owing to the fact that the WSM database contains only very sparse information on in situ stress from the Arabian Plate, we conducted a public-domain literature review to scout for and extract such information. We found 23 publications from which we generated a regional database consisting of 143 in situ stress data points extracted from a variety of publications addressing topics and themes that require information on the present-day in situ stress state. These stress indicators include wellbore breakouts, drilling-induced fractures and recent geologic structures. They reflect the present-day in situ stress orientation. Table 1 provides an overview of the references from which the stress information was extracted, categorized by country, the number of data points and the corresponding WSM quality.

Stress indicators

Useful stress indicators include drilling-induced wellbore breakouts and tensile fractures, together with geologic structures (igneous intrusions) as described in detail by Zoback (2010). Geological indicators include structures from the Quaternary age. Tensile fractures, igneous dykes and volcanic alignments grew parallel to the S_{Hmax} direction at the time when these features formed (Sperner *et al.* 2003).

The extracted stress data in Table 1 come from circular histograms (rose diagrams), tabular data and azimuths plotted on maps of the respective area. Herein, we list and explain the procedure used to select the data (Fig. 2):

- (1) Acoustic image log data from wells in North Kuwait fields (Abdali, Bahrah, Dhabi, Mutriba, Raudhatain, Ratqa, Sabriyah and Umm Niqa) show a general trend of N40°E–N50°E (Cretaceous formation) and N20°E–N90°E (Jurassic formation). The S_{Hmax} azimuths variability from Cretaceous to Jurassic formation is explained by the presence of the Gotnia Salt that, due to its rheologic nature, decouples in situ stress below from that above (Al-Ammar et al. 2012; Perumalla et al. 2014).
- (2) The stress state in Qatar's North Field located in the Arabian Gulf is constrained using data

Table 1. List of countries and associated publications from which we extracted present day *in situ* stress orientation plotted in Figure 2b

Country	Number of S_{Hmax} data	WSM quality	References
Saudi Arabia	57	B, C	Ameen et al. (2010) Ameen (2014) Ameen (2016) Ameen (2019) Raba'a et al. (2007) Coleman et al. (1983) Xu et al. (2015)
Kuwait	22	A, B, C, D	Perumalla <i>et al.</i> (2014)
UAE	22	A, C	Franquet <i>et al.</i> (2018)
			Noufal and Obaid (2016)
			Pham et al. (2020)
Iraq	7	B, C, D	Awdal et al. (2013) Alkamil et al. (2018) Mohammed et al. (2018) Almalikee and Sen (2021) Gilchrist et al. (2020) Soroush et al. (2011)
Jordan	1	C	Diabat (2009)
Oman	29	C	Filbrandt et al. (2006)
Qatar	1	В	Jonaghani et al. (2019)
Bahrain	1	C	Al-Muftah <i>et al.</i> (2009)
Yemen	2	С	Barton <i>et al.</i> (2010) Murray and Montgomery (2014)
Turkey/Iran	1	В	Mokhoori et al. (2021)

The World Stress Map (WSM) quality ranking scheme adopted from Heidbach et al. (2016).

- from three gas wells. The S_{Hmax} azimuth trends NE–SW (Jonaghani *et al.* 2019).
- (3) Borehole image analysis from 16 wells of the Ahmadi carbonate reservoir, located in the
- Bahrain Field, indicates that the S_{Hmax} has a NW–SE orientation (Ali *et al.* 2009).
- (4) The present-day stress condition of Oman has been extensively studied in the north-central

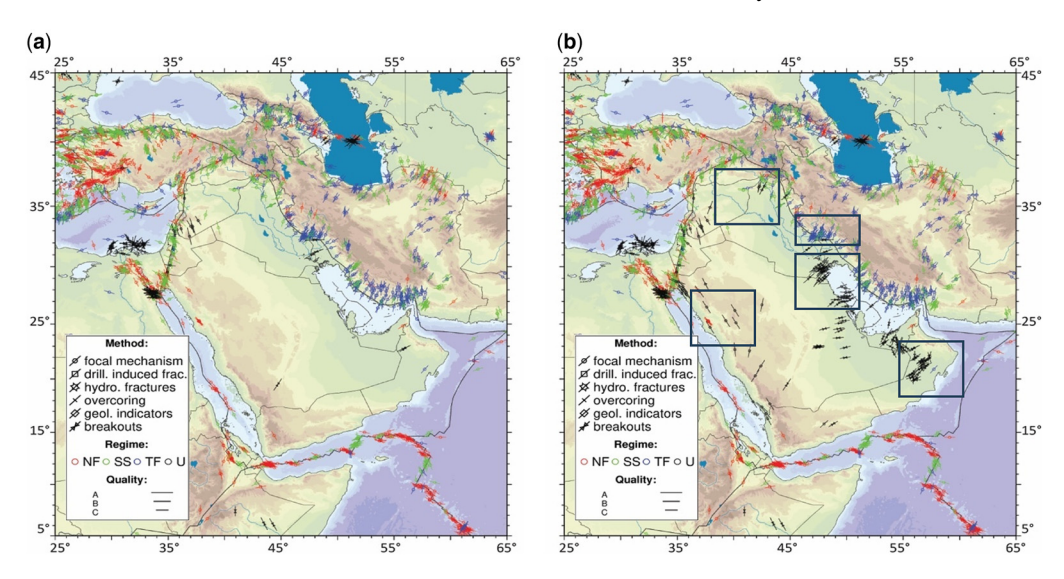


Fig. 2. World Stress Map (WSM) of the Arabian Plate region, containing: (a) A–C quality data; (b) A–C quality data combined with our new database. Black rectangles enclose areas used as validation points for our numerical implementation. Source: Heidbach *et al.* (2016).

- region. The overall trend of the S_{Hmax} is NE–SW, with slight variations in regions with active faults. In these regions, the *in situ* stress state is reoriented from NW–SE to east–west. In the Khazzan gas field, the regional S_{Hmax} trend is NE–SW (Filbrandt *et al.* 2006).
- (5) The geomechanical model in the Raoq Field in North Yemen suggests NE–SW S_{Hmax} azimuths. Furthermore, studies from the Say'um Masila Basin region indicate N55°E S_{Hmax} azimuths (Barton *et al.* 2010; Murray and Montgomery 2014).
- (6) Stress inversion from 277 earthquake focal mechanisms in NW Iran–SE Turkey results in S_{Hmax} trending N158°E (Mokhoori *et al.* 2021).

Note that we assessed the extracted *in situ* stress data's quality according to the rigorous ranking system of the WSP, excluding data ranked as qualities D and E. Consequently, we based our numerical validation on only 143 data points corresponding to qualities A–C.

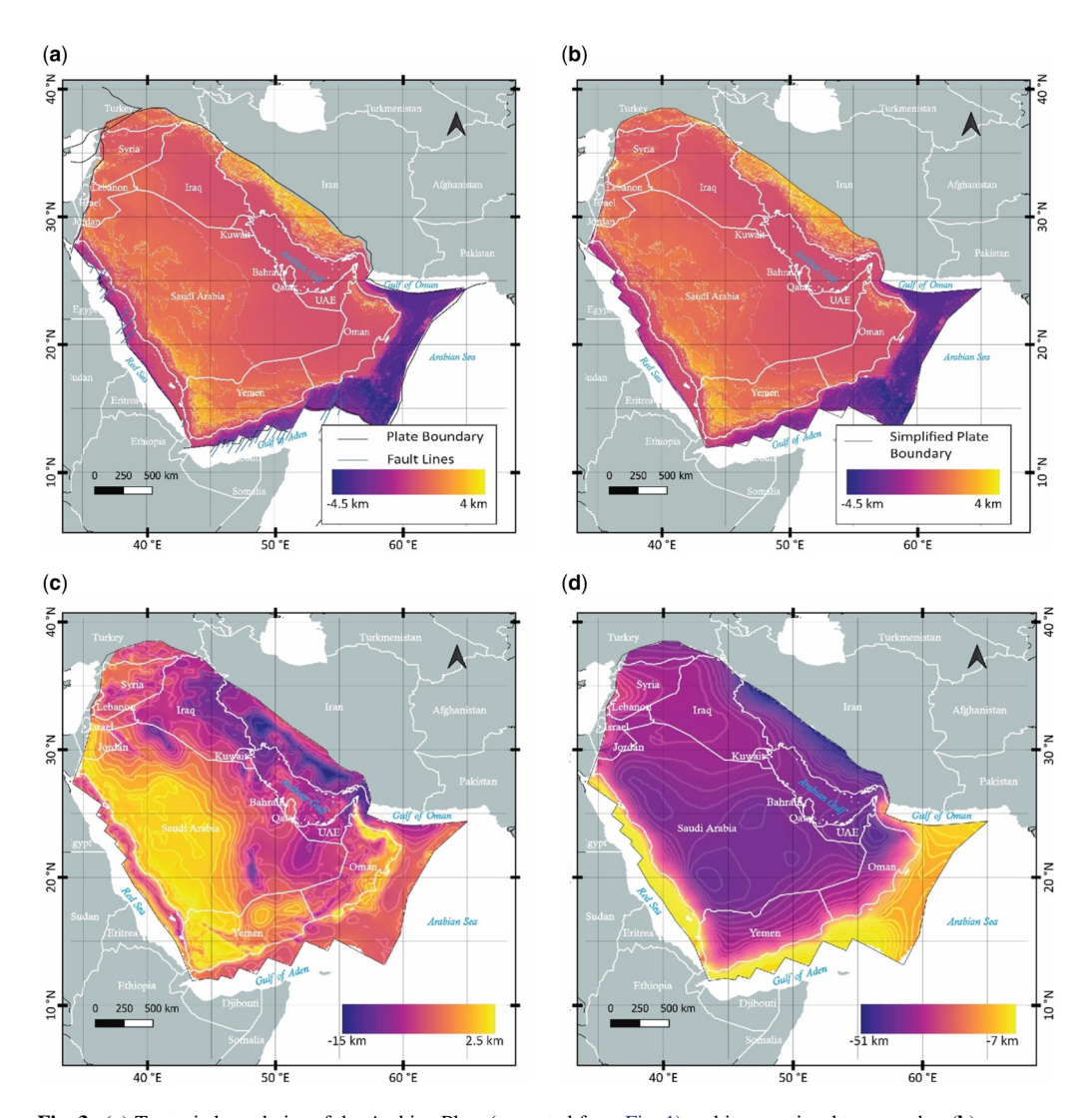


Fig. 3. (a) Tectonic boundaries of the Arabian Plate (extracted from Fig. 1) and its associated topography; (b) our simplification of the plate boundaries considers the mesh resolution in finite element scheme; (c) depth map of the crystalline basement; (d) depth map of the Moho discontinuity.

Numerical model

Figure 3 shows the study area of this work and the plate boundaries. We simplify the fault systems in the Red Sea and Gulf of Aden areas as the spacing between them is below the model resolution (Fig. 3b). The Red Sea and Gulf of Aden areas are mainly related to model discretization that allows accurate and affordable computational simulation runs. Although these fault systems might significantly contribute to the deformation process, their mechanical responses have a local impact only. Consequently, in this work, which considers present-day in situ stress patterns on a plate scale, we do not include fault systems. Furthermore, we model the Arabian Plate as a dry, elastic rock solid. Therefore, we do not account for pore pressure changes (e.g.

resulting from petroleum activities in oil or gas fields) to model the overall mechanical behaviour of the Arabian Plate. We acknowledge that there may be such localized effects within certain reservoirs, but for the purposes of this paper, we chose to focus on the plate-scale deformation. Finally, the area encompassed by the boundaries in Figure 3b is extruded vertically to create the 3D model volume.

To reduce the Arabian Plate geological complexity, we build a 3D watertight subsurface model that includes the oceanic domains (i.e. the Red Sea, the Gulf of Aden and the Arabian Sea oceans). It is composed of three main compartments: the sedimentary cover, the crystalline basement and the upper mantle. In Figure 3a, we use the freely available GEBCO grid, which provides the topography and the bathymetry surfaces of the model (Kapoor 1981).

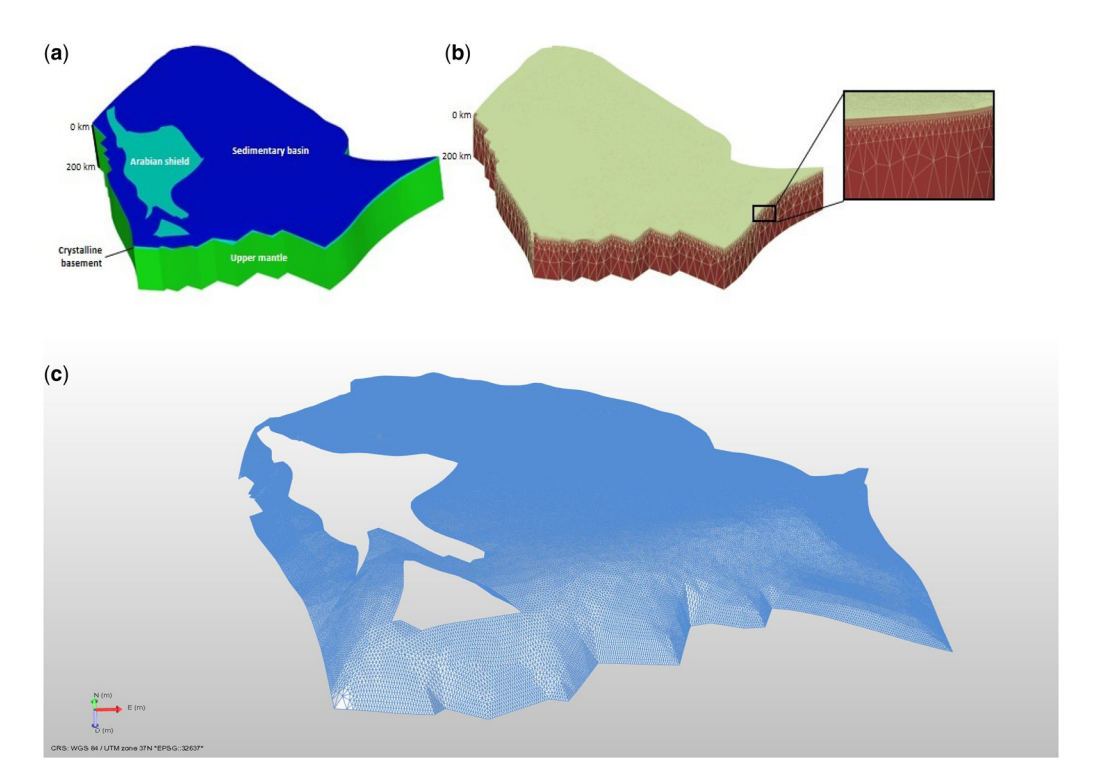
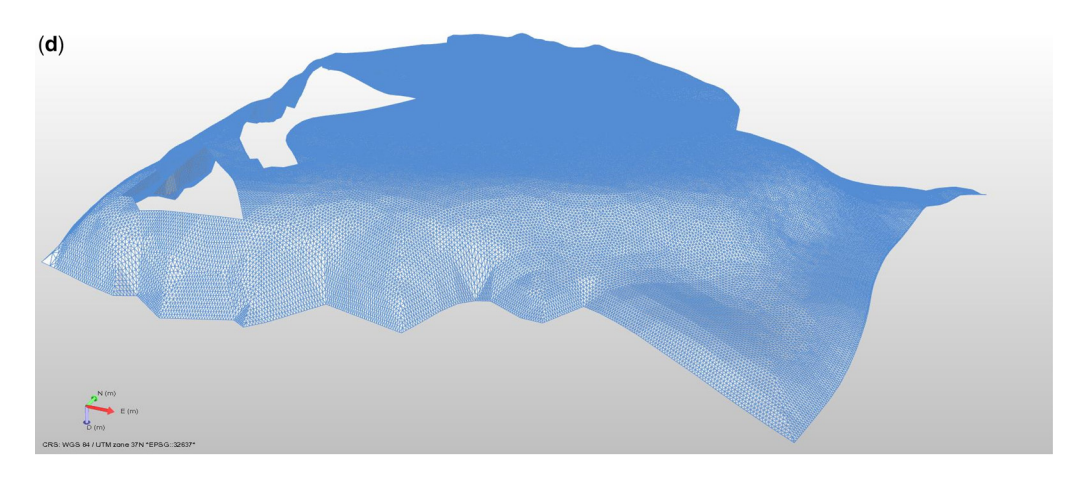
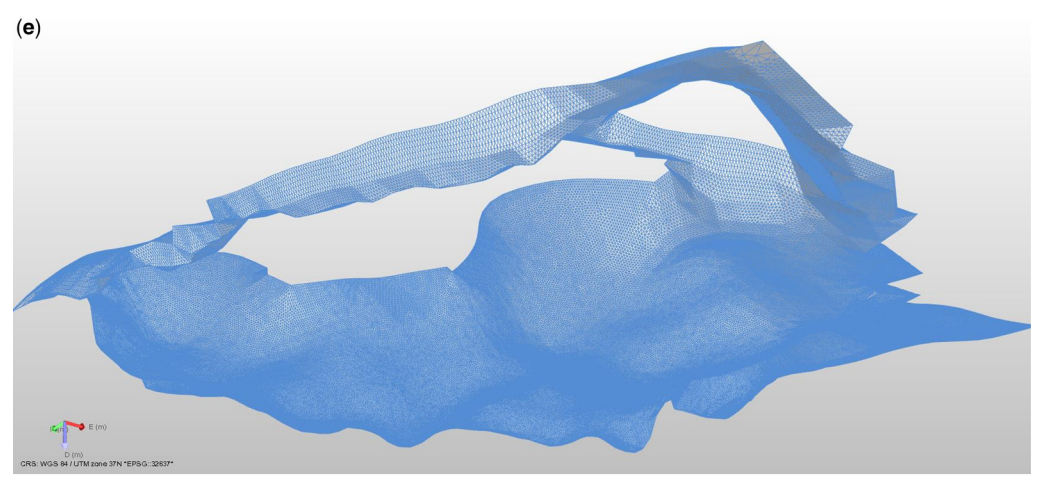


Fig. 4. (a) Subsurface model of the Arabian Plate. Four surfaces were used to build this model, from bottom to top: a flat bottom surface at 200 km (which is below the isostatic compensation depth), the Moho discontinuity, the top basement and the topography. These four surfaces, together with the Arabian Plate boundaries, encompass a watertight model composed of three compartments: the sedimentary cover (dark blue), the crystalline basement (light blue) and the upper mantle (green). Vertical exaggeration x2. (b) Finite element mesh after discretizing the Arabian Plate subsurface model used in this work (Fig. 4a). Notice that the size of the elements in the vertical direction become thicker from top to bottom. This strategy reduces the computational time to solve the problem while avoiding distorted elements. Vertical exaggeration x2. (c-e) These provide different viewpoints of the basin geometry. The implemented finite element mesh ensures a thorough representation of the basin's geometry, facilitating precise finite element calculations. (f) This illustrates the discretized basement geometry using finite elements. While our primary focus was on the basin model, it remains essential to accurately represent the entire model geometry to prevent distorted finite elements, which can lead to unreliable finite element calculations.

Arabian Plate in situ stress modelling





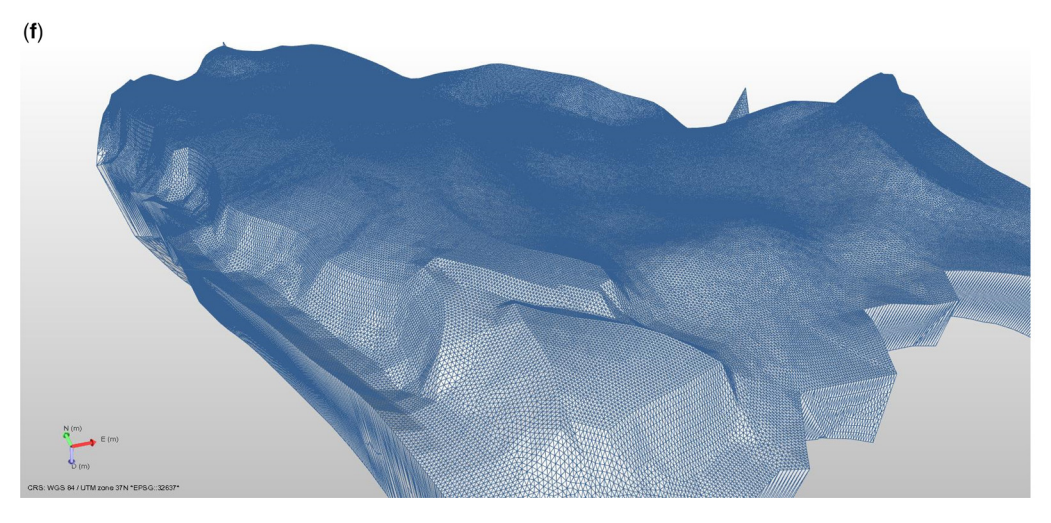


Fig. 4. Continued.

Moreover, we use updated versions of the top crystalline basement and crust-mantle (Moho) discontinuity depth maps. To build crystalline basement and the Moho discontinuity depth maps (Fig 3c, d), we compiled isopach and isobath maps, geological sections, seismic refraction profiles, seismic stations and proprietary depth-migrated seismic reflection profiles available from the literature (Kaban et al. 2016, 2019). These data were geo-referenced, digitized and interpolated using QGIS 3.22 software and Move 2020.1 software: Arabian Platform, Geert et al. (2001), Kaviani et al. (2020); Gulf of Oman, Ali et al. (2020), Ninkabou et al. (2021), Tarapoanca et al. (2010), Weidle et al. (2022); Arabian Sea: Exxon (1985); Gulf of Aden, Autin et al. (2008), Cochran (1981), d'Acremont et al. (2005), Gillard et al. (2021), Laske et al. (2013), Leroy et al. (2012), Nonn et al. (2017, 2019), Watremez et al. (2011); Red Sea, Al-Damegh et al. (2005), Blanchette et al. (2018), Davison et al. (1998), Doornenbal et al. (1991), Gaulier et al. (1988), Hansen et al. (2007), Makris et al. (1991). In line with Goteti et al. (2021), we adopted a model configuration with the bottom layer situated at a depth of 200 km, which is positioned beneath the isostatic compensation level for the Arabian Plate. This choice ensures that mechanical loading resulting from topographic and bathymetric changes becomes negligible at the fixed bottom layer.

In order to capture the Arabian Plate subsurface geometry with sufficient resolution in our numerical model, we use a finite element approach to solve the force balance partial differential equation (see equation A8). The finite element method has been extensively used to model plate-scale deformation, providing accurate numerical results for complex geometries (Buchmann 2008; van-der-Zee et al. 2011; Reiter and Heidbach 2014; Ahlers et al. 2021). Thus, we discretize the subsurface model, as illustrated in Figure 4a, using tetrahedral finite elements. Tetrahedral finite element meshes allow modelling of complex geometries while having affordable computational runs. Our finite element mesh is composed of 3.1 million C3D4 Abagus general-purpose tetrahedral elements. The discretization resolution plays a major role in the accuracy of the finite element solution. When using linear functions for regions with steep elevation gradients, sufficiently small discretization is required to capture these variations (e.g. the transition from the Arabian Shield region with exposed basement to the Arabian Platform sedimentary cover). We refine our finite element mesh using a central node remeshing strategy to capture the thickness variations in the sedimentary basin. Figure 4b portrays our model discretization. This mesh geometry and configuration do not possess several distorted elements, which would result in unrealistic numerical

solutions. Figure 4c–e shows the basin thickness variations from three distinct perspectives alongside the basement structure (Fig. 4f).

The mesh quality is assessed using established metrics, including aspect ratio, shape factor and trifaced corner angles, to ensure the reliability and accuracy of the finite element simulations. The colour-coded representation in Figure 5 highlights the mesh quality across the model. Unshaded areas indicate elements that conform to the defined quality criteria, while areas with deviations from the criteria are depicted in yellow. Notably, only few elements exhibit these deviations, predominantly localized near the corners of the model. These minor deviations from the quality metrics do not compromise the overall integrity of the finite element results. It is important to emphasize that most of the mesh elements meet the quality standards, underscoring the robustness of the mesh for simulating deformation processes. The observed deviations in mesh quality can be attributed to the inherent challenges posed by the transition zones, especially structural heterogeneities. However, we emphasize that the impact of these deviations on the accuracy of the simulations is minimal, given their localized nature.

Figure 6 outlines the key stages of a comprehensive stress modelling workflow. Beginning with the Arabian Plate subsurface model and material properties, it then defines initial stress state and boundary conditions. These inputs feed into a geomechanical model, followed by its discretization into finite elements. The process involves solving force balance equations, culminating in the post-processing of stress results for the stress modelling analysis.

We use the ABAQUSTM/Standard implementation to solve the linear static and elastic analysis (Abaqus 2011). Material properties for the linear elastic compartments are listed in Table 2. Without loss of generality, we consider isotropic materials throughout the Arabian Plate. Therefore, the material properties do not change spatially. Furthermore, we adopt a stress notation where compressional stresses are positive and negative stresses indicate tension. To calculate principal stress orientations, the linear static analysis following equation (A8) must be solved using either displacement or force boundary conditions.

An essential aspect of modelling *in situ* stress azimuths in rock volumes is to account for as many sources of deformation as possible. In this study, we consider the following:

 Lateral boundary forces between different plates. In the case of Arabian Plate, we find six main plate interactions: Arabian— Anatolian, Arabian—Sinai, Arabian—Nubian, Arabian—Somalian. Arabian—Indian and

Arabian Plate in situ stress modelling

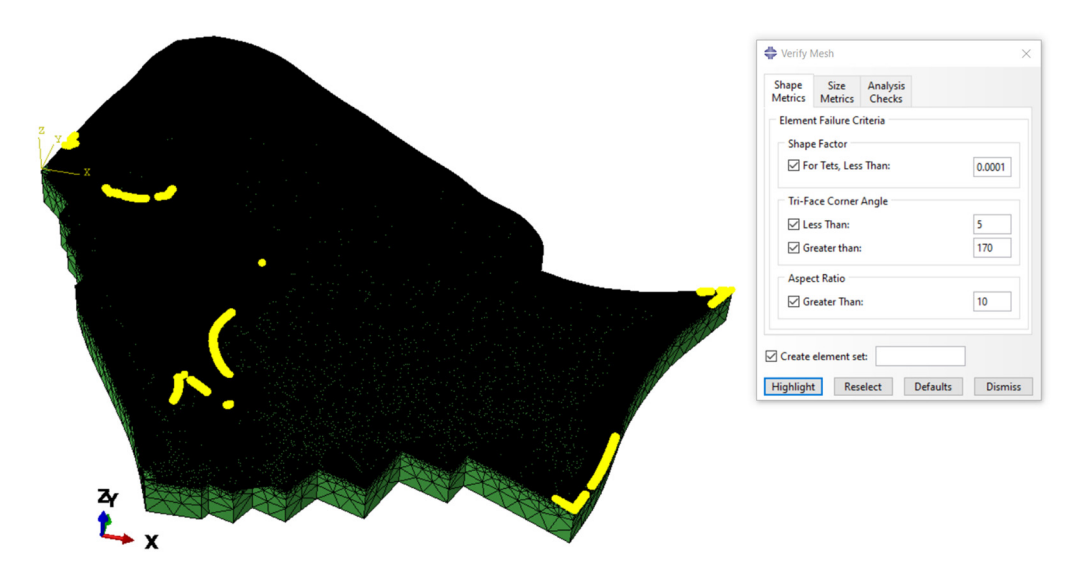


Fig. 5. Colour-coded representation of finite element mesh quality assessment for the Arabian Plate. No shaded areas indicate elements meeting quality criteria, while deviations are highlighted in yellow.

Arabian–Eurasian (see Fig. 1 to locate these plates). We excluded the Arabian–Danakil interaction as their boundary is not yet well constrained.

- (2) Gravitational potential energy differences caused by lateral density variations, e.g. transition from the Arabian Shield to the Arabian Platform sedimentary cover.
- Equilibrium between model geometry and state of initial geostatic stress.

Nonetheless, it is worth mentioning that additional contributions to the mechanical responses in rocks exist, such as thermal stresses, pore pressure distributions, viscoelastic effects and residual stresses, which are not considered in this work. The latter assumptions do not markedly change our simulation results from the observed data. Hence, this work is still valid and representative under such modelling considerations. Along the lateral plate boundaries, we impose accumulative displacement boundary conditions inferred from the most current plate velocity model (Goteti et al. 2021; Viltres et al. 2022). Several present-day plate boundary interactions define the plate velocities. The spreading rates are 16–10 mm yr⁻¹ in the Red Sea (Chu and Gordon 1998) and c. 30 mm yr $^{-1}$ (Courtillot 1980) in the Gulf of Aden, with an average northward drift of the plate of 20-30 mm yr⁻¹ (Bird et al. 2002). The present-day convergence rates between Arabia and Eurasia are 19–23 mm yr⁻¹ (McClusky et al. 2003). We choose several points and calculate corresponding linear velocities using Euler vectors and locations. Moreover, we guarantee that the selected sites can be captured by the mesh resolution.

Figure 7a shows the angular rotations $\dot{\omega}$ together with their locations. Based on the various velocities around the plate, we divide the plate boundary into six segments, each with a constant Euler vector and location. Figure 7b shows the GPS velocity model proposed by Viltres et al. (2022). Using the linear relation between velocity and time, we calculate the respective displacement boundary conditions. We choose a time span of 100 kyr to estimate cumulative deformation. Assuming a linear relation for velocity changes over 100 kyr is feasible since the plate has not moved substantially over this time period (ArRajehi et al. 2010; Viltres et al. 2022). For the uppermost boundary model, we do not constrain the displacement field since the Earth's surface serves as a free boundary. For the bottom layer, roller boundary conditions in the vertical direction are applied. Vertical roller boundary conditions constrain the model from vertical movement while allowing horizontal motion.

Accounting for the initial stress state in the rock volume is challenging. We assume the rock volume is in quasi-static equilibrium with *in situ* stresses, gravitational loading, tectonics and stress-assisted thermal deformation, to name a few. In our framework, we estimate the initial stress state using the model geometry, gravity and *in situ* stresses. Thus, before imposing displacement boundary conditions, we initialize the stress state in the model using the geostatic analysis procedure in ABAQUSTM/Standard. This step involves the roller boundary

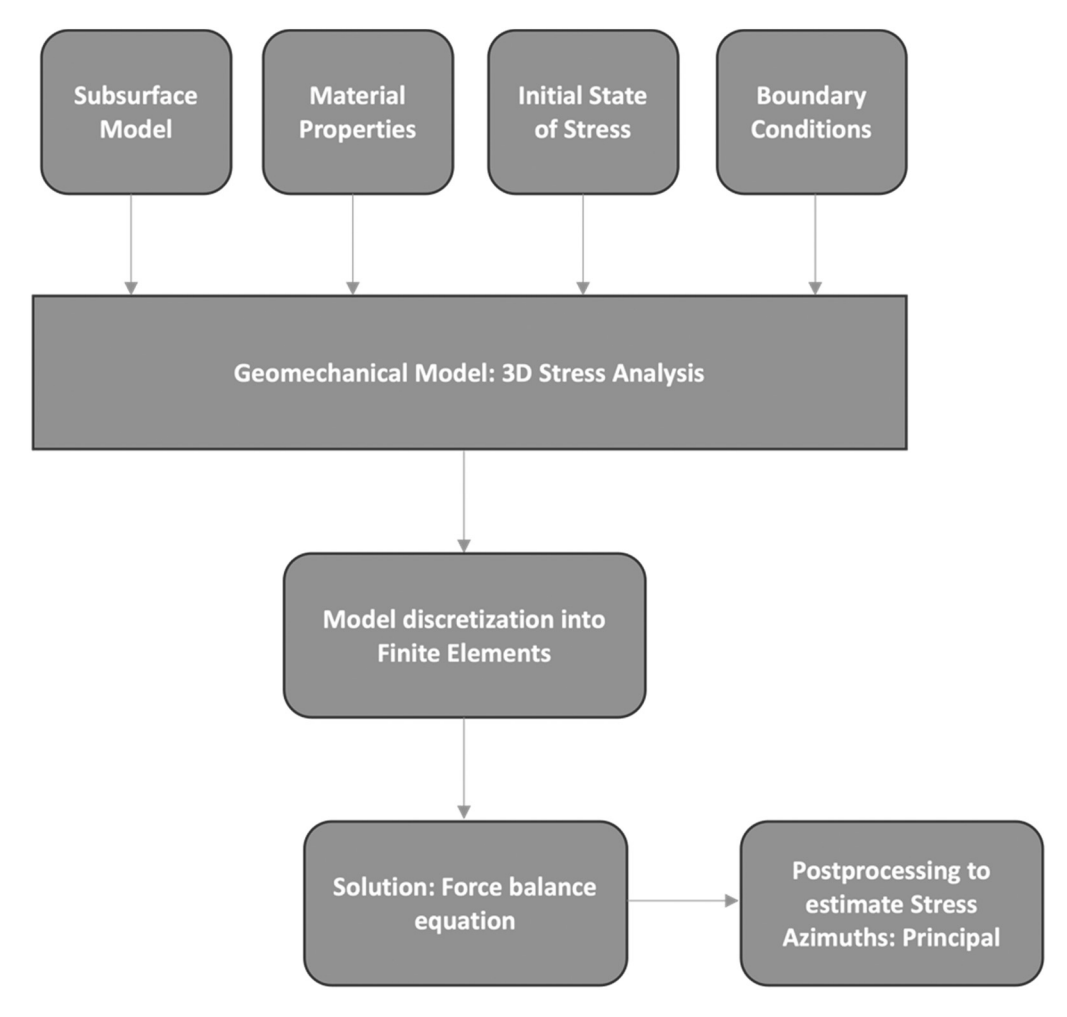


Fig. 6. Stress modelling workflow: GPS velocities are used to calculate displacement boundary conditions, which are then employed in the geomechanical framework solved with finite elements.

conditions and gravity to seek equilibrium with the model geometry and initial *in situ* stresses, preventing unrealistic elastic compaction caused by the gravitational loading. As a result, we can model the

Table 2. Material parameters used in the numerical mode

Compartment	Density (kg m ⁻³)	Young's modulus (GPa)	Poisson's ratio (-)
Sedimentary basin	2100	20	0.25
Basement	2300	55	0.1
Upper mantle	3350	140	0.25

Source: Goteti et al. (2021).

kinematic behaviour of the rock volume during a time span while accounting for a pre-stressed solid. Our numerical simulations use a vertical stress gradient of 24.5 MPa $\rm km^{-1}$ and ratio of horizontal to vertical effective stresses of 0.8 (Goteti *et al.* 2021). We post-process our simulation to showcase the maximum horizontal stress azimuths. Furthermore, we assume that the vertical stress, $S_{\rm V_{\rm c}}$ is a principal stress direction.

Results and discussion

Figure 8 presents the initial S_{Hmax} azimuths, located at 4 km depth below sea-level, before imposing boundary conditions. The non-uniform pattern arises from the combined effects of the applied initial stress state and gravitational forces. However, to accurately

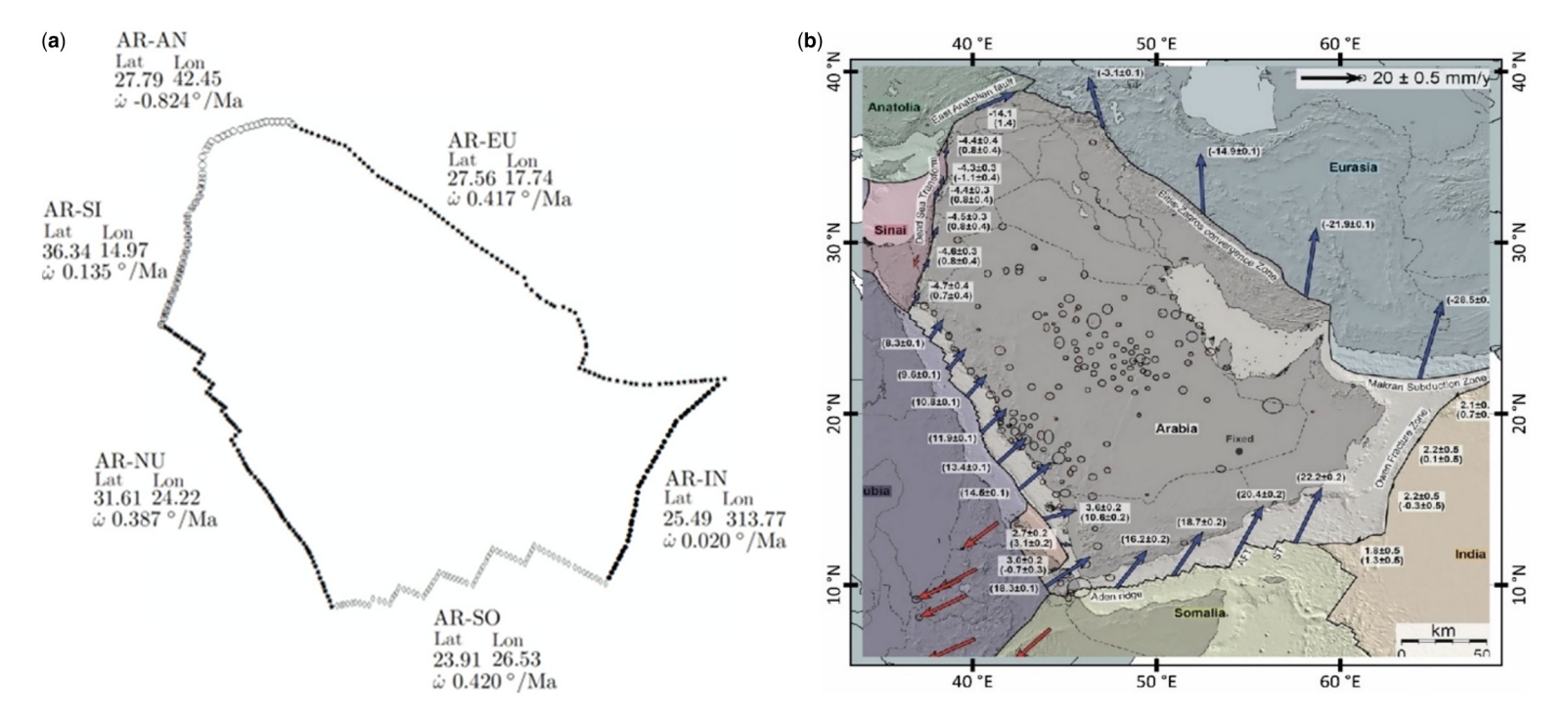


Fig. 7. (a) GNSS-derived angular velocities. AR–NU, Arabian–Nubian; AR–SO, Arabian–Somalian; AR–IN, Arabian–Indian; AR–EU, Arabian–Eurasian; AR–AN, Arabian–Anatolian; AR–SI, Arabian–Sinai. (b) Map illustrating the motion of the Arabian Plate at its plate boundaries. Blue arrows indicate the estimated relative motion, which is crucial for calculating cumulative displacements. Source: Viltres *et al.* (2022).

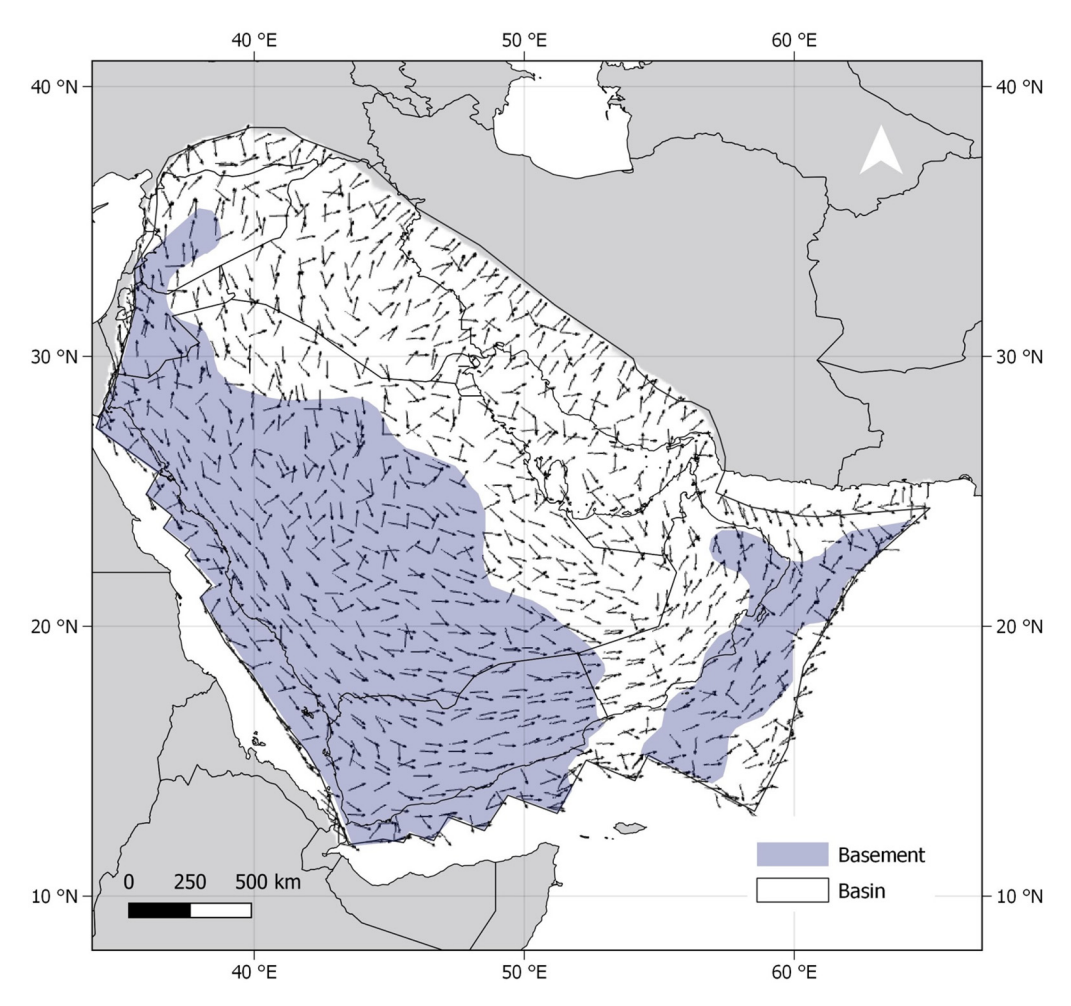


Fig. 8. Initial S_{Hmax} azimuths after geostatic step. The geostatic step models the equilibrium state of model geometry influenced by gravitational forces and the initial stress state. During this step, gravity loading and initial stress state are applied to the model, allowing it to settle into its stable configuration, zero displacement field. The results obtained from the geostatic step serve as the initial conditions for subsequent loading analyses.

replicate the current S_{Hmax} azimuths within the Arabian Plate, additional adjustments involving pushing and pulling at the six boundaries of the domain are necessary to correctly modulate the displacement field. This geostatic procedure is typically employed as a first initial step in geomechanics analysis, during which gravity loads are applied to arrive at an initial stress state. In this step, the loads and initial stresses must equilibrate, resulting in zero deformations, which is the case with our model. Figure 9 shows the initial model displacements after the geostatic step.

In Figure 10, S_{Hmax} azimuths result from the combination of the initial stress state (initial stress state, gravitational loading and model geometry)

with the stress induced by applying displacement boundary conditions (derived from Fig. 7). Figure 11 shows the displacement field magnitude that leads to the observed S_{Hmax} azimuths. We conducted a sensitivity analysis to pinpoint the model parameters that significantly influence S_{Hmax} azimuths in the model. Our findings indicate that the most critical parameter is the displacement field applied across the six different boundaries. Figure 12 presents the influence of three displacement fields on S_{Hmax} azimuths, employing black arrows to represent the displacement field orientations. In Figure 12a, the displacement field orientation is predominantly north—south in the Red Sea, Gulf of Aden, and Owen Fault areas. Conversely, in the Dead Sea Fault region,

Arabian Plate in situ stress modelling

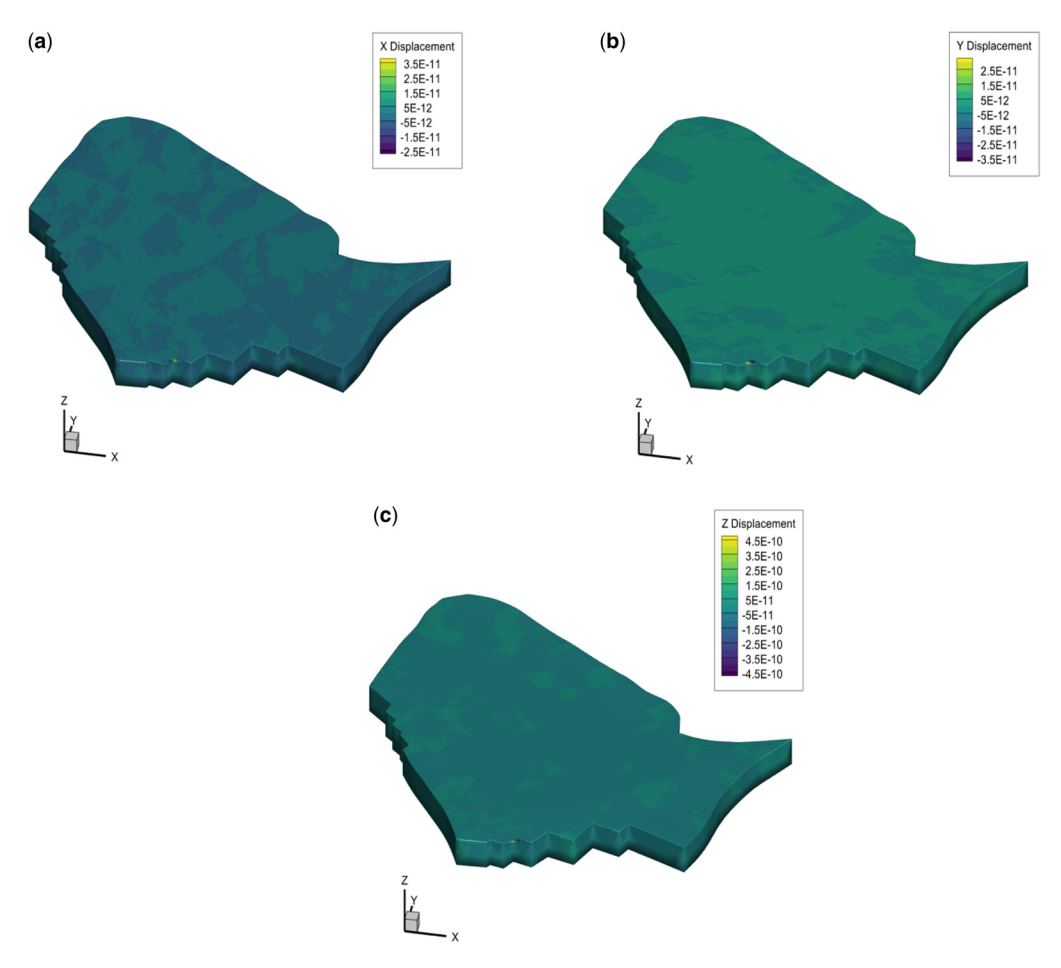


Fig. 9. The displacement field following the geostatic step exhibits zero displacementmagnitudes in the following directions: (a) X; (b) Y and (c) Z.

the orientation mainly follows a NNW-SSW pattern. These orientations result in an east-west orientation of the $S_{\mbox{\scriptsize Hmax}}$ azimuths across most of the plate. In the Iraq region, there is a notable shift in the S_{Hmax} azimuths, transitioning from a NE-SW to an NNE-SSW orientation. Close to the boundary of the Zagros fold belt, the S_{Hmax} azimuths take on a NW-SE orientation. In Figure 12b, the displacement field orientations are primarily north-south in the Red Sea, NNW-SSE in the Gulf of Aden and east-west in the Owen Fault region. Conversely, within the Dead Sea Fault region, the orientation shifts from an east-west to a WNW-ESE pattern, resulting in an overall east-west alignment of the S_{Hmax} azimuths across most of the tectonic plate. In the Iraq region, there is a notable shift in the S_{Hmax} azimuths, transitioning from NE-SW to NNE-SSW. Near the boundary of the Zagros fold belt, the S_{Hmax} azimuths

take on a NW–SE orientation. Additionally, a stress rotation is observed in the transition from the Red Sea to the Gulf of Aden, shifting from north–south to NW–SE, and subsequently returning to north–south in the transition from the Gulf of Aden to the Owen Fault region. It is important to note that the earlier displacement field does not accurately represent plate motion, leading to the observed deviations in stress data. In contrast, as depicted in Figures 10 and 11, the displacement field calculated from GPS velocities yields a stress azimuth pattern that closely aligns with the observed data, highlighting a robust agreement between simulation results and real-world observations.

Notably, different applied displacement fields can yield the same S_{Hmax} azimuth pattern. Therefore, to constrain the model and its displacement boundary conditions further, it is necessary to calibrate

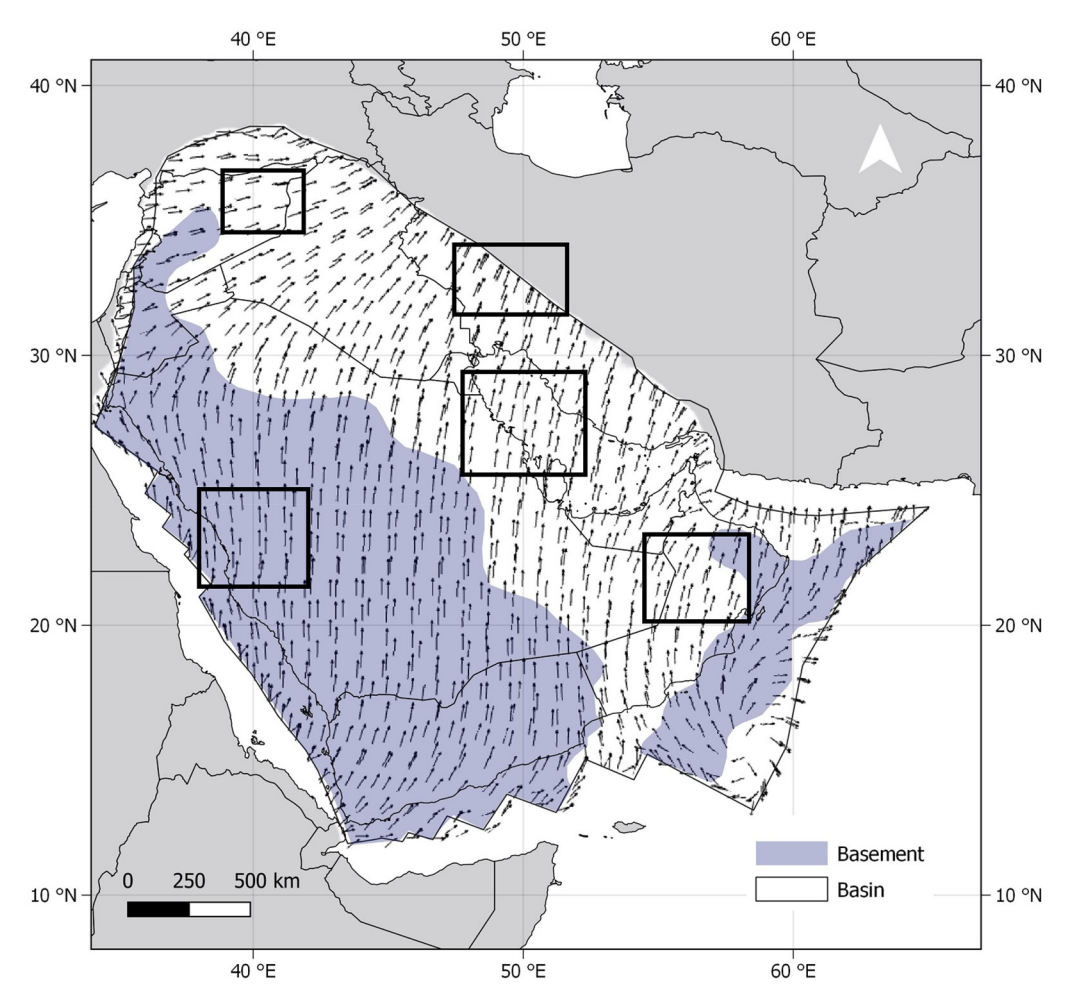


Fig. 10. S_{Hmax} azimuth at 4 km depth after imposing displacement boundary conditions at several locations on the Arabian Plate. Black rectangles enclose areas used as validation points for our numerical implementation. These areas are also highlighted in Figure 2.

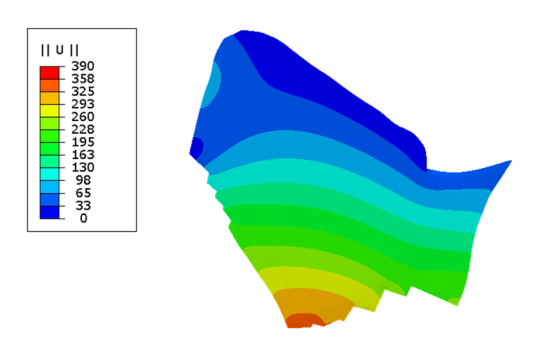


Fig. 11. The displacement field, which determines the validated S_{Hmax} azimuths, is computed using GPS velocities.

stress magnitudes. However, given the lack of published stress magnitude data (and those we found are associated with large uncertainties) across the Arabian region (in particular in Saudi Arabia) such a calibration process is currently not feasible. Previous work on plate-scale deformation modelling constructs the solid geometry, such that the horizontal boundary's faces are perpendicular to the azimuths of the maximum principal compressive stresses (Altmann et al. 2014; Reiter and Heidbach 2014; Ziegler et al. 2016; Ziegler and Heidbach 2021). Consequently, applying perpendicular displacement boundary conditions captures the stress azimuths naturally. In our approach, we model the Arabian Plate using the real plate boundary shape and related crustal deformation (using the most current GPS

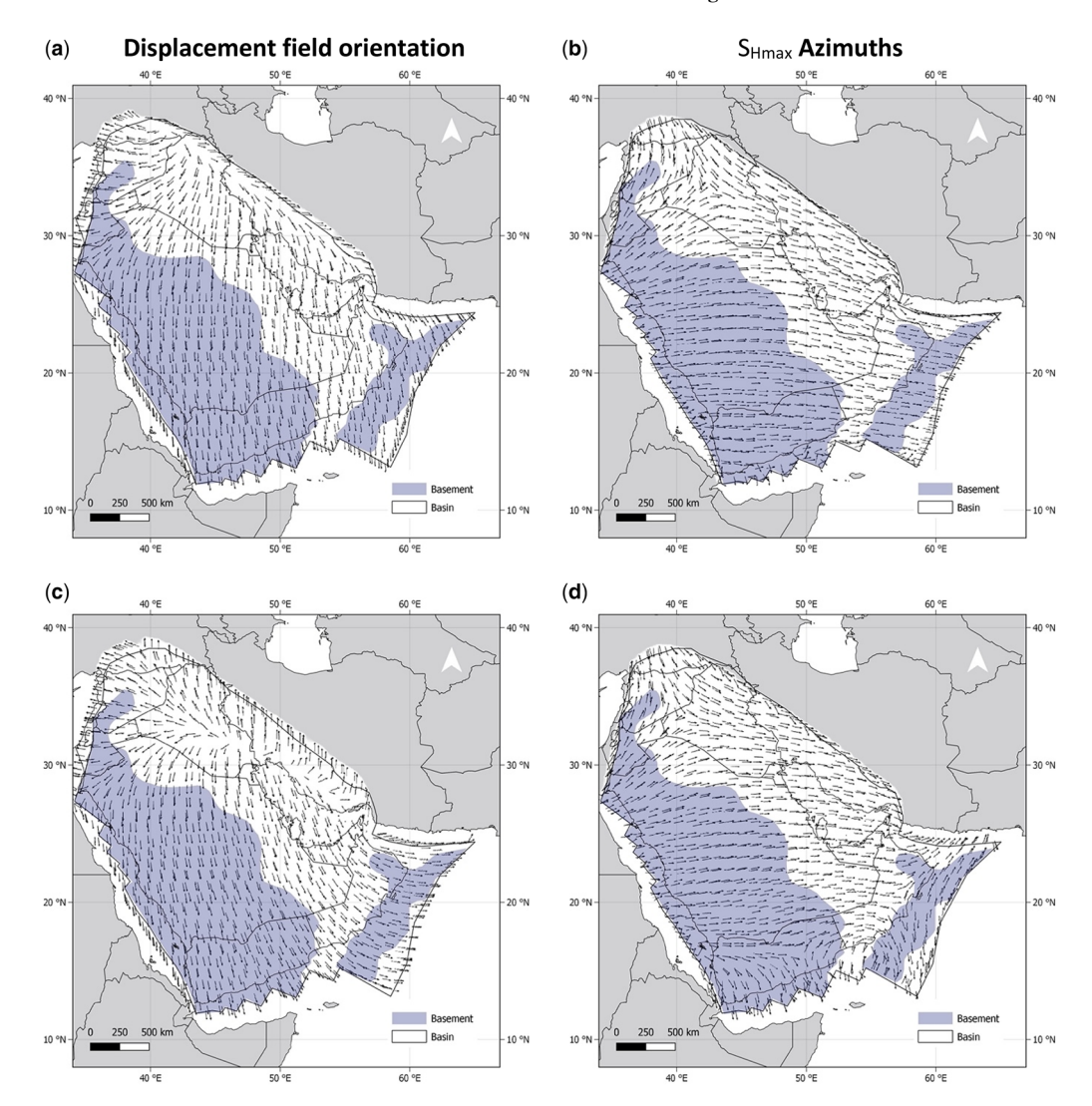


Fig. 12. The sensitivity analysis underscores that the key parameter in our 3D geomechanical model is the displacement field applied at the model boundaries. We showcase two distinct displacement fields alongside their corresponding S_{Hmax} azimuths. (a) Displacement field leads to S_{Hmax} north–south S_{Hmax} orientations in the Red Sea, Gulf of Aden and Owen Fault areas, while transitioning to an NNE–SSW pattern in the Iraq region and NW–SE near the Zagros Fold Belt boundary (b). (c) Displacement field leads to S_{Hmax} north–south orientations in the Red Sea, NNW–SSE in the Gulf of Aden, and east–west in the Owen Fault region, with a shift to a WNW–ESE pattern in the Dead Sea Fault region (d). These two displacement field orientations do not lead to observed S_{Hmax} azimuths.

data) to capture the impact of the plate geometry in the stress field orientations.

GPS velocities used in this work suggest counterclockwise rotation for the Arabian Plate (see e.g. fig. 7b in; Viltres *et al.* 2022). When translating from linear velocities to displacements, the deformation leads to slightly deviated north–south azimuths of the maximum principal horizontal compressive stresses for most of the Arabian Plate. As previously noted, the resulting pattern considers the initial stress state, which is influenced by gravitational loading as well. We notice that by increasing the number of points to evaluate the linear velocities along the plate boundary, namely the sampling, the simulation results replicate the observed data more accurately, suggesting the dependency on both the imposed amount of deformation and their spatial distribution along the plate boundary. To emphasize again, the

sampling also depends upon the resolution of the finite element mesh, since these points must coincide with nodal points. In this study, we use all nodal points for imposing boundary conditions as inferred from their corresponding angular rotations and Euler poles. The data points for stress azimuths used in this work are within the range of 0–12 km. We chose to represent the simulated stress azimuths at 4 km depth since the model within the 0–12 km range does not undergo significant changes. Furthermore, this depth falls within the range accessed by industry for energy extraction processes.

The simulation results show NE-SW SHmax azimuths in northeastern Saudi Arabia and Kuwait. NE S_{Hmax} azimuths dominate the Arabian Gulf region. The collected data, as depicted in Figure 2b, reveal S_{Hmax} azimuths that closely align with the calculated S_{Hmax} azimuths in Figure 10. It is worth noting that minor deviations between the calculated S_{Hmax} azimuths and the observed data fall within the range of uncertainties associated with breakouts and drilling-induced fractures. Farther north, from the Dead Sea transform area to the Arabian-Anatolian boundary in Iraq's western area, S_{Hmax} azimuths rotate counterclockwise from NNW-SSE to NW-SE. We observed the same pattern between the calculated S_{Hmax} azimuths in Figure 10 and the collected S_{Hmax} azimuth data in Figure 2b. This behaviour highlights the influence of the pinned boundary along the collision zone and the displacement field variations along the Arabian-Anatolian boundary. S_{Hmax} azimuths in the Dead Sea transform region trend NW-SE and NNW-SSE.

Again, a pinned boundary, but also gravitational loading, in the Zagros Mountain Range, results in a S_{Hmax} azimuths shift. In the southwestern region of the plate, azimuths change due to the high-relief topography in conjunction with large displacement imposed in the eastern part of the Gulf of Aden relative to the southwestern part of the Red Sea boundary (intersection between two different plate boundaries, Arabia–Africa and Arabia–Somalia). Figure 11 illustrates that the applied displacement field exhibits the greatest magnitude within this region. Therefore, the azimuths rotate counterclockwise from ENE–WSW to north–south.

Our simulation results allow the understanding and study of the current S_{Hmax} azimuths in the Arabian Plate. To a large extent, the model results suggest NE–SW S_{Hmax} azimuths in northeastern Saudi Arabia and Kuwait, while the Dead Sea transform areas show NW–SE to NNW–SSE azimuths, and the rest of the plate is characterized by predominant north–south S_{Hmax} azimuths.

The modelling of the current *in situ* stress azimuths in the Arabian Plate presented in this work uses a simplified geometry of the brittle lithosphere

in the sense that the present model does not account for fault systems, sub-basin boundaries, lateral facies changes, and changes in material properties and rheologies. Such discontinuities contribute significantly to the local perturbations of the *in situ* stress field. Nevertheless, the overall stress field is mostly controlled by gravitational potential energy arising from density variations together with tectonic processes described in the 'Numerical model' section.

We apply the displacement field perpendicular to the boundary faces, meaning that the imposed displacement field is not a function of depth. The latter is relevant to capture deformation processes at subduction zones and seafloor spreading. Moreover, in our simulations, we do not include the slow creeping motion of the continental lithosphere base caused by convection currents carrying heat from the interior to the Earth's surface.

Our modelling highlights how the stress orientation pattern in the Arabian Plate results from the superposition of gravitational loading and tectonism. We acknowledge that various factors, including mechanical discontinuities (e.g. faulting at various scales), basin morphology, human activities (such as production or/and injection) and salt domains, can markedly affect stress conditions locally. Consequently, strategic and accurate stress measurements are required to calibrate deformation models at a plate-scale level, albeit they are currently unavailable for the Arabian Plate. Despite this limitation, our numerical analysis demonstrates that, for most of the plate, stress patterns are primarily governed by tectonic interactions along plate boundaries and gravitational loading.

Using a finite element model of the Arabian Plate, Goteti et al. (2021) also derived an in situ stress map of the Arabian Plate. Their model results agree in some measures with the available stress data for the Arabian region. As we find in our study, the model geometry plays a significant role when applying boundary conditions inferred from GPS velocities. In this work, we provide a comprehensive geometry of the Arabian Plate, which favours capturing the stress behaviour for essential regions such as Western Iraq, Oman, Kuwait and the Dead Sea transform. We use the most recent GPS velocity model available for the Arabian region, which allows us to constrain the model more accurately (Viltres et al. 2022). The validation process involved in this work compares simulated stress azimuths with stress azimuth information obtained from various sources in the literature, including drilling-induced fractures, volcanic vents and breakout data, as highlighted in the section 'The present-day stress pattern in the Arabian Plate: compilation of published data to augment the WSM database'. Although not ubiquitous across the modelled region, the data nonetheless validate our modelling framework and make the

resulting stress azimuths more robust. However, it is essential to acknowledge the need for additional measurements – not only present-day *in situ* stress orientation but also magnitudes. Despite the abundance of drilling projects conducted throughout the Arabian region, we found that there was a marked lack of publicly available stress magnitude data. This represents a significant gap in our current understanding. Should such data become available, they not only have the potential to refine our understanding of the current *in situ* stress and associated models (regionally and locally), but also reduce uncertainties and manage risks in order to optimize resource exploration, exploitation and other subsurface activities.

Summary and conclusions

We present a static present-day in situ stress - S_{Hmax} azimuth - model of the Arabian Plate to elucidate ongoing tectonic processes and plate boundary interactions. The modelling framework is based on a finite element method in conjunction with a plate velocity model. The finite element method allows us to build a comprehensive 3D representation of the Arabian Plate, focusing on the Arabian Shield, sedimentary basin and upper mantle geometries. Further, we use a recently published plate velocity model to evaluate the current deformation process at plate boundaries. The combination of the finite element model and the plate velocity model facilitates the study of the deformation field in the Arabian Plate at plate and regional scales. Finally, we conduct an extensive literature review on available in situ stress data, providing new data points that complement those already in the WSM Project. The main results are summarized as follows:

- The plate velocities used in this work constrain the amount of deformation at plate boundaries when imposing accumulative displacement boundary conditions.
- (2) The Arabian Plate shows appreciable stress azimuths variability caused by topography changes, plate boundary intersections and plate boundary interactions.
- (3) Across the transition from the Arabian Shield to the basin, the azimuths rotate from northsouth to NNE-SSW and north-south to NW-SSE in several regions, particularly those close to the model boundaries.
- (4) The effect of the Zagros collision zone, modelled as pinned boundary conditions, has a significant impact on the stress field since the azimuths rotate toward the western part of the plate.
- (5) We found 143 in situ stress azimuth data points extracted from wellbore breakouts, drilling-

- induced fractures and volcanic vents from a variety of publications. These new data points serve as validation points in this work as well as in future numerical studies.
- (6) It is crucial for future research to prioritize acquiring and releasing already existing stress azimuth and magnitude data to calibrate and further refine our understanding of the Arabian Plate's present day in situ stress field.

Acknowledgements The authors wish to thank King Abdullah University of Science and Technology (KAUST) for supporting this work and are grateful to Prof. Oliver Heidbach and Dr Moritz Ziegler for their fruitful comments and insights. The authors thank Sander De Jong from Baker Hughes for providing feedback on implementing the finite element mesh. The authors also thank Baker Hughes for providing licenses to the subsurface modelling software JewelSuiteTM.

Competing interests The authors declare that they have no known competing financial interests or personal relationships that could have appeared to influence the work reported in this paper.

Author contributions SPC: conceptualization (lead), data curation (lead), formal analysis (lead), investigation (lead), methodology (lead), software (lead), validation (lead), visualization (lead), writing – original draft (lead); AD: data curation (supporting), investigation (supporting), visualization (supporting); GB: investigation (supporting), visualization (supporting), writing – review & editing (supporting); TF: conceptualization (supporting), formal analysis (supporting), investigation (supporting), supervision (lead), writing – review & editing (lead).

Funding This project was funded by Ali Al-Naimi Petroleum Engineering Research Center of King Abdullah University of Science and Technology.

Data availability Data sharing is not applicable to this article as no datasets were generated or analysed during the current study.

Appendix A: Mathematical model

We assume the Arabian Plate behaves as a linear elastic continuum body. Deformation across the solid boundaries and body forces, i.e. plate boundary interactions and gravitational loading, drive the stress-generation process. We follow the notation as suggested by Gurtin *et al.* (2010). Thus, a time-dependent deformation field $\chi: \mathbf{B} \times]0$, $\mathbf{T}[\to \mathbf{B}_t \subset \varepsilon$ defines the particle motion from a configuration \mathbf{B} onto another configuration \mathbf{B}_t in the Euclidean space ε for the time span]0, $\mathbf{T}[$. Henceforth,

we refer to **B** as a reference configuration and **X** as material particles. Conversely, the spatial particles **x** in the current configuration **B**, are given by $\mathbf{x} = \chi(\mathbf{X}, t)$. The material and spatial particles definition allows defining a displacement field as follows:

$$\mathbf{u} = \mathbf{x}(\mathbf{X}, \ t) - \mathbf{X} \tag{A1}$$

together with the deformation gradient:

$$\mathbf{F} = \nabla \chi = \nabla \mathbf{u} + \mathbf{I} \tag{A2}$$

where **I** corresponds to the second-order identity tensor. Moreover, the Jacobian of the deformation field reads:

$$J = \det \mathbf{F} > 0. \tag{A3}$$

Using the change of variables theorem, we relate infinitesimal area and volume elements in the reference and current configurations such that:

$$da = \mathbf{F}^{-T} da_R \tag{A4}$$

$$dv = Jdv_R.$$
 (A5)

To close the set of equations, we use linear and angular momentum, and mass balances in the form of partial differential equations to describe the particle's motion as the solid endures deformation caused by external forces such gravity, and displacement boundary conditions. Thereby, let $\mathbf{P} \subset \mathbf{B}$ be a control volume in the reference configuration in conjunction with its counterpart in the spatial configuration $\mathbf{P}_t \subset \mathbf{B}$. Due to solid mass conservation, we define ρ and ρ_0 as the solid density in the current and reference configuration, respectively. Consequently, the solid mass balance is:

$$\int_{P} \rho \, dv - \int_{P} \rho_0 \, dv_R = 0. \tag{A6}$$

The localized version of equation (A6) expresses the local solid mass conservation. Following Cauchy's theorem, the traction on a surface area $da \subset S$ with pointwise outwards normal \mathbf{n} is $\mathbf{t} = \sigma \mathbf{n}$, which renders:

$$\int_{S} \mathbf{t} \, da + \int_{P} \mathbf{b} \, dv_{R} = \mathbf{0}. \tag{A7}$$

By means of the divergence theorem, we arrive at:

$$\int_{P_r} Div \, \boldsymbol{\sigma} \, da + \int_{P} \mathbf{b} \, dv_R = \mathbf{0}. \tag{A8}$$

We focus on quasi-static processes, i.e. we neglect all inertial effects and set the spatial velocity as constant. The localized version of equation (A8) is then:

$$Div \mathbf{\sigma} + \mathbf{b} = \mathbf{0}. \tag{A9}$$

Herein, the body force b corresponds to the gravitational loading such that $\mathbf{b} = \rho \mathbf{g}$. In linear elasticity, the stress tensor σ is proportional to strain tensor such that:

$$\sigma = C\epsilon$$
. (A10)

We use Hooke's stress-strain relation, therefore:

$$\sigma_{ij} = \frac{E}{1+\nu} \left[\epsilon_{ij} + \frac{\nu}{1-2\nu} \, \delta_{ij} \, \epsilon_{kk} \right] \tag{A11}$$

where E and v represent Young's modulus and Poisson's ratio, respectively. Note that Einstein summation convention applies to equation (A11). The symmetric nature of Cauchy's stress tensor arises from the angular momentum conservation balance, which implies that equation (A8) must always hold. Most importantly, there exists a coordinate system where the shear stresses vanish, leading to the principal stresses.

References

Abaqus, G. 2011. Abaqus 6.11. Dassault Systemes Simulia Corporation. Providence, RI, USA, 3.

Ahlers, S., Henk, A. et al. 2021. 3D crustal stress state of Germany according to a data-calibrated geomechanical model. Solid Earth, 12, 1777–1799, https://doi.org/ 10.5194/se-12-1777-2021

Ahmed, M.S., Finkbeiner, T. and Kanan, A.M. 2007. Using geomechanics to optimize field development strategy of deep gas reservoir in Saudi Arabia. Asia Pacific Oil and Gas Conference and Exhibition.

Ahmed, S., Khan, K., Omini, P., Abdulaziz, A., Ahmed, M., Yadav, A.S. and Mohiuddin, M.A. 2014. An integrated drilling and geomechanics approach helps to successfully drill wells along the minimum horizontal stress direction in Khuff Reservoirs. 30th Abu Dhabi International Petroleum Exhibition and Conference, ADIPEC 2014: Challenges and Opportunities for the Next 30 Years. OnePetro, Society of Petroleum Engineers.

Al-Ammar, N., Hussain, R., Mulyono, R., Al-Fares, A., Al-Kandary, A., Al-Naeimi, R. and Perumalla, S. 2012. Regional In-Situ Stress in Northern Kuwait-Implications for the oil Industry. Paper presented at the SPE Kuwait International Petroleum Conference and Exhibition, Kuwait City, Kuwait, SPE-163366-MS.

Al-Damegh, K., Sandvol, E. and Barazangi, M. 2005. Crustal structure of the Arabian plate: New constraints from the analysis of teleseismic receiver functions. *Earth and Planetary Science Letters*, 231, 177–196, https://doi.org/10.1016/j.epsl.2004.12.020

Ali, A.-M., Kumar, K. et al. 2009. Integrated reservoir connectivity study of Ahmadi fractured reservoir in Bahrain Field. Paper presented at the SPE/EAGE Reservoir Characterization & Simulation Conference, Abu Dhabi, United Arab Emirates. Society of Petroleum Engineers. Paper number cp-170.

Ali, M., Watts, A., Searle, M., Keats, B., Pilia, S. and Ambrose, T. 2020. Geophysical imaging of ophiolite

- structure in the United Arab Emirates. *Nature Communications*, **11**, 1–10, https://doi.org/10.1038/s41467-019-13993-7
- Alkamil, E., Abbood, H., Flori, R. and Eckert, A. 2018. Case study of wellbore stability evaluation for the Mishrif Formation, Iraq. *Journal of Petroleum Science and Engineering*, 164, 663–674, https://doi.org/10.1016/j.petrol.2018.01.018
- Almalikee, H.S. and Sen, S. 2021. Present-day stress field and stress path behaviour of the depleted Mishrif reservoir from the super-giant Zubair oilfield, Iraq – a geomechanical case study. *Journal of African Earth Sciences*, 184, 104–381, https://doi.org/10.1016/j. jafrearsci.2021.104381
- Al-Muftah, A., Kumar, K. et al. 2009. Integrated Reservoir Connectivity Study of Ahmadi Fractured Reservoir in Bahrain Field. SPE 125400, SPE/EAGE Reservoir Characterization and Simulation Conference, 19–21 October 2009, Abu Dhabi, UAE.
- Al-Shijbi, Y., El-Hussain, I., Deif, A., Al-Kalbani, A. and Mohamed, A.M.E. 2019. Probabilistic Seismic Hazard Assessment for the Arabian Peninsula. *Pure and Applied Geophysics*, 176, 1503–1530, https://doi. org/10.1007/s00024-018-2033-4
- Altmann, J.B., Müller, B., Müller, T., Heidbach, O., Tingay, M. and Weißhardt, A. 2014. Pore pressure stress coupling in 3D and consequences for reservoir stress states and fault reactivation. *Geothermics*, 52, 195–205, https://doi.org/10.1016/j.geothermics.2014.01.004
- Ameen, M.S. 2014. Fracture and in-situ stress patterns and impact on performance in the Khuff structural prospects, eastern offshore Saudi Arabia. *Marine and Petroleum Geology*, 50, 166–184, https://doi.org/10.1016/ j.marpetgeo.2013.10.004
- Ameen, M.S. 2016. Fracture modes in the Silurian Qusaiba Shale Play, Northern Saudi Arabia and their geotechnical implications. *Marine and Petroleum Geology*, 78, 312–355, https://doi.org/10.1016/j.marpetgeo.2016. 07.013
- Ameen, M.S. 2019. Borehole Imaging of Natural Fractures and Stress Indicators in the Jurassic Carbonaye Shale Plays, Eastern Saudi Arabia. We KN 05, Sixth EAGE Shale Workshop, 28 April –1 May 2019, Bordeaux, France
- Ameen, M.S., Buhidma, I.M. and Rahim, Z. 2010. The function of fractures and in-situ stresses in the Khuff reservoir performance, onshore fields, Saudi Arabia. AAPG Bulletin, 94, 27–60, https://doi.org/10.1306/ 06160909012
- ArRajehi, A., McClusky, S. et al. . 2010. Geodetic constraints on present-day motion of the Arabian Plate: implications for Red Sea and Gulf of Aden rifting. Tectonics, 29, https://doi.org/10.1029/2009TC0 02482
- Autin, J., Leroy, S. et al. 2008. Continental break-up history of a poor magnetic margin from seismic reflection (NE Gulf of Aden margin, offshore Oman). Geophysical Journal International, 180, 501–519, https://doi.org/10.1111/j.1365-246X.2009.04424.x
- Awdal, A.H., Braathen, A., Wennberg, O.P. and Sherwani, G.H. 2013. The characteristics of fracture networks in the Shiranish Formation of the Bina Bawi Anticline; comparison with the Taq Taq Field, Zagros, Kurdistan,

- NE Iraq. *Petroleum Geoscience*, **19**, 139–155, https://doi.org/10.1144/petgeo2012-036
- Barton, C., Moos, D., Montgomery, D. and Whiteley, P. 2010. Shear Stimulation of a Basement Fractured Reservoir âÄithe Raoq Field, Yemen. Second EAGE Middle East Tight Gas Reservoirs Workshop, Exploration & Development Strategies, 12–15 December 2010, Manama, Bahrain, cp-244.
- Bird, P., Kagan, Y.Y. and Jackson, D.D. 2002. Plate tectonics and earthquake potential of spreading ridges and oceanic transform faults. *In*: Stein, S. and Freymueller, J.T. (eds) *Plate Boundary Zones*, https://doi.org/10.1029/GD030p0203
- Blanchette, A.R., Klemperer, S.L., Mooney, W.D. and Zahran, H.M. 2018. Two-stage Red Sea rifting inferred from mantle earthquakes in Neoproterozoic lithosphere. *Earth and Planetary Science Letters*, **497**, 92–101, https://doi.org/10.1016/j.epsl.2018.05.048
- Bosworth, W., Huchon, P. and McClay, K. 2005. The red sea and gulf of aden basins. *Journal of African Earth Sciences*, **43**, 334–378, https://doi.org/10.1016/j.jafrearsci.2005.07.020
- Buchmann, T. 2008. 3D multi-scale finite element analysis of the present-day crustal state of stress and the recent kinematic behaviour of the northern and central Upper Rhine Graben. [PhD-Thesis – Research external, graduation internal, Vrije Universiteit Amsterdam]. Logos Verlag Berlin GmbH.
- Chu, D. and Gordon, R.G. 1998. Current plate motions across the Red Sea. *Geophysical Journal International*, 135, 313–328, https://doi.org/10.1046/j.1365-246X. 1998.00658.x
- Cochran, J.R. 1981. The Gulf of Aden: structure and evolution of a young ocean basin and continental margin. *Journal of Geophysical Research: Solid Earth*, **86**, 263–287, https://doi.org/10.1029/JB086iB01p00263
- Coleman, R.G., Gregory, R.T. and Brown, G.F. 1983. Cenozoic Volcanic Rocks of Saudi Arabia. United States Department of the Interior, Geological Survey, Open-File Report 83-788.
- Cornet, F., Helm, J., Poitrenaud, H. and Etchecopar, A. 1997. Seismic and aseismic slips induced by large-scale fluid injections. *In: Seismictry Associated with Mines, Reservoirs and Fluid Injections*. Pageoph Topical Volumes. Birkhäuser, Base, https://doi.org/10.1007/978-3-0348-8814-1_12
- Courtillot, V.E. 1980. Opening of the Gulf of Aden and Afar by progressive tearing. *Physics of the Earth and Planetary Interiors*, **21**, 343–350, https://doi.org/10.1016/0031-9201(80)90137-5
- d'Acremont, E., Leroy, S. *et al.* 2005. Structure and evolution of the eastern Gulf of Aden conjugate margins from seismic reflection data. *Geophysical Journal International*, **160**, 869–890, https://doi.org/10.1111/j. 1365-246X.2005.02524.x
- Davison, I., Tatnell, M., Owen, L., Jenkins, G. and Baker, J. 1998. Tectonic geomorphology and rates of crustal processes along the Red Sea margin, north-west Yemen. In: Purser, B.H. and Bosence, D.W.J. (eds) Sedimentation and Tectonics in Rift Basins Red Sea: Gulf of Aden. Springer, Dordrecht, https://doi.org/10.1007/978-94-011-4930-3_32
- De Lamotte, D.F. and Leturmy, P. 2014. The structural map of the Arabian Plate and surrounding areas. *Episodes*

- Journal of International Geoscience, 37, 111–114, https://doi.org/10.18814/epiiugs/2014/v37i2/005
- Diabat, A.A. 2009. Structural and stress analysis based on fault-slip data in the Amman area, Jordan. *Journal of African Earth Sciences*, **54**, 155–162, https://doi.org/ 10.1016/j.jafrearsci.2009.03.011
- Doornenbal, J.C., DeGroot, P.F.L., Saif, S.M. and Schroot, B.M. 1991. Geology and hydrocarbon potential of the Tihama Basin, Republic of Yemen. Geology and hydrocarbon potential of the Tihama Basin, Republic of Yemen. Paper presented at the Middle East Oil Show, Bahrain, November 1991, https://doi.org/10. 2118/21393-MS
- Exxon, 1985. Tectonic Map of the World, Mapping Project, Scale 1:5000,000, 20 Panels. American Association of Petroleum Geologists, Tulsa, OK, USA.
- Filbrandt, J.B., Al-Dhahab, S. *et al.* 2006. Kinematic interpretation and structural evolution of North Oman, Block 6, since the Late Cretaceous and implications for timing of hydrocarbon migration into Cretaceous reservoirs. *GeoArabia*, **11**, 97–140, https://doi.org/10.2113/geoarabia110197
- Franquet, J., Shaver, M., Edwards, E., Al Neyadi, A., Noufal, A. and Khairy, H. 2018. Microfrac in-situ stress measurements for drilling and completion design in Middle-Lower Cretaceous reservoirs in a giant field of Abu Dhabi, UAE Offshore. Paper presented at the Abu Dhabi International Petroleum Exhibition & Conference, Abu Dhabi, UAE, November 2018, https://doi.org/10.2118/193004-MS
- Fuchs, K. and Müller, B. 2001. World stress map of the Earth: a key to tectonic processes and technological applications. *Naturwissenschaften*, 88, 357–371, https://doi.org/10.1007/s001140100253
- Gaucher, E., Schoenball, M., Heidbach, O., Zang, A., Fokker, P.A., van Wees, J.-D. and Kohl, T. 2015. Induced seismicity in geothermal reservoirs: a review of forecasting approaches. *Renewable and Sustainable Energy Reviews*, 52, 1473–1490, https://doi.org/10.1016/j.rser.2015.08.026
- Gaulier, J., Le Pichon, X. *et al.* 1988. Seismic study of the crust of the northern Red Sea and Gulf of Suez. *Tectonophysics*, **153**, 55–88, https://doi.org/10.1016/0040-1951(88)90007-8
- Geert, K., Afifi, A.M., Al-Hajri, S.A. and Droste, H.J. 2001.
 Paleozoic stratigraphy and hydrocarbon habitat of the Arabian Plate. *GeoArabia*, 6, 407–442, https://doi.org/10.2113/geoarabia0603407
- Gilchrist, C.J.D., Cosgrove, J.W. and Parmassar, K.J. 2020. Critically stressed fractures: analysis of the Shaikan Field, Kurdistan Region of Iraq. *Journal of the Geological Society*, *London*, 177, 1315–1328, https://doi.org/ 10.1144/jgs2019-136
- Gillard, M., Leroy, S., Cannat, M. and Sloan, H. 2021. Margin-to-margin seafloor spreading in the eastern Gulf of Aden: a 16 Ma-long history of deformation and magmatism from seismic reflection, gravity and magnetic data. Frontiers in Earth Science, 9, https:// doi.org/10.3389/feart.2021.707721
- Goteti, R., Alzayer, Y., Baek, H. and Han, Y. 2021. Regional in-situ stress prediction in frontier exploration and development areas: insights from the first-ever 3D geomechanical model of the Arabian Plate. Paper presented at the SPE Middle East Oil & Gas Show and

- Conference, event cancelled, November 2021, https://doi.org/10.2118/204866-MS
- Gurtin, M.E., Fried, E. and Anand, L. 2010. The Mechanics and Thermodynamics of Continua. Cambridge University Press, Cambridge.
- Hansen, S.E., Rodgers, A.J., Schwartz, S.Y. and Al-Amri, A.M. 2007. Imaging ruptured lithosphere beneath the Red Sea and Arabian Peninsula. *Earth and Planetary Science Letters*, 259, 256–265, https://doi.org/10. 1016/j.epsl.2007.04.035
- Heidbach, O. and Ben-Avraham, Z. 2007. Stress evolution and seismic hazard of the Dead Sea Fault System. Earth and Planetary Science Letters, 257, 299–312, https:// doi.org/10.1016/j.epsl.2007.02.042
- Heidbach, O., Barth, A., Müller, B., Reinecker, J., Stephansson, O., Tingay, M. and Zang, A. 2016. WSM quality ranking scheme, database description and analysis guidelines for stress indicator. World Stress Map Technical Report 16-01, GFZ German Research Centre for Geosciences, http://doi.org/10. 2312/wsm.2016.001
- Heidbach, O., Rajabi, M. et al. 2018. The World Stress Map database release 2016: crustal stress pattern across scales. Tectonophysics, 744, 484–498, https://doi.org/ 10.1016/j.tecto.2018.07.007
- Heidbach, O., Rajabi, M., Reiter, K. and Ziegler, M.O. 2019. World Stress Map. In: Sorkhabi, R. (ed.) Encyclopedia of Petroleum Geoscience. Encyclopedia of Earth Sciences Series. Springer, Cham., https://doi.org/10.1007/978-3-319-02330-4_195-1
- Hergert, T., Heidbach, O., Reiter, K., Giger, S. and Marschall, P. 2015. Stress field sensitivity analysis in a sedimentary sequence of the Alpine foreland, northern Switzerland. *Solid Earth*, 6, 533–552, https://doi.org/10.5194/se-6-533-2015
- Johnson, P.R. and Woldehaimanot, B. 2003. Development of the Arabian-Nubian Shield: Perspectives on accretion and deformation in the northern East African Orogen and the assembly of Gondwana. *Geological Society, London, Special Publications*, 206, 289–325, https://doi.org/10.1144/GSL.SP.2003.206.01.15
- Jonaghani, H.H., Manshad, A.K. et al. 2019. Fracture analysis and in situ stress estimation of a gas condensate field in Persian Gulf using FMI and DSI image logs. SN Applied Sciences, 1, 1–14, https://doi.org/10.1007/s42452-019-1466-4
- Kaban, M.K., El Khrepy, S. and Al-Arifi, N. 2016. Isostatic model and isostatic gravity anomalies of the Arabian plate and surroundings. *Pure and Applied Geophysics*, 173, 1211–1221, https://doi.org/10.1007/s00024-015-1164-0
- Kaban, M.K., El Khrepy, S., Al-Arifi, N. and Petrunin, A.G. 2019. Upper-mantle density structure beneath the Congo Basin from inversion of satellite gravity and topography data. *Geophysical Journal International*, 219, 945–959, https://doi.org/10.1093/gji/ggz303
- Kapoor, D. 1981. General bathymetric chart of the oceans (GEBCO). Marine Geodesy, 5, 73–80, https://doi. org/10.1080/15210608109379408
- Kaviani, A., Paul, A. et al. 2020. Crustal and uppermost mantle shear wave velocity structure beneath the Middle East from surface wave tomography. Geophysical Journal International, 221, 1349–1365, https://doi. org/10.1093/gji/ggaa075

- Konert, G., Afifi, A.M., Al-Hajri, S.A. and Droste, H.J. 2001. Paleozoic stratigraphy and hydrocarbon habitat of the Arabian plate. *GeoArabia*, 6, 407–442, https:// doi.org/10.2113/geoarabia0603407
- Laske, G., Masters, G., Ma, Z. and Pasyanos, M. 2013. Update on CRUST1. 0-A 1-degree global model of Earth's crust. Geophysical Research Abstracts, 15, 2658
- Leroy, S., Razin, P. et al. 2012. From rifting to oceanic spreading in the Gulf of Aden: a synthesis. Arabian Journal of Geosciences, 5, 859–901, https://doi.org/ 10.1007/s12517-011-0475-4
- Makris, J., Henke, C.H., Egloff, F. and Akamaluk, T. 1991.
 The gravity field of the Red Sea and East Africa. *Tectonophysics*, 198, 369–381, https://doi.org/10.1016/0040-1951(91)90161-K
- McClusky, S., Reilinger, R., Mahmoud, S., Ben Sari, D. and Tealeb, A. 2003. GPS constraints on Africa (Nubia) and Arabia plate motions. *Geophysical Journal International*, 155, 126–138, https://doi.org/10.1046/j.1365-246X.2003.02023.x
- Moeck, I., Backers, T. et al. 2011. Fault reactivation potential as a critical factor during reservoir stimulation. First Break, 29, 80, https://doi.org/10.3997/1365-2397. 2011014
- Mohammed, H.Q., Abbas, A.K. and Dahm, H.H. 2018. Wellbore instability analysis for Nahr Umr Formation in Southern Iraq. ARMA 18–916, 52nd US Rock Mechanics/Geomechanics Symposium held in Seattle, 17–20 June 2018, Washington, USA.
- Mokhoori, A.N., Rahimi, B. and Moayyed, M. 2021. Active tectonic stress field analysis in NW Iran-SE Turkey using earthquake focalmechanism data. *Turkish Journal of Earth Sciences*, 30, 235–246, https://doi.org/10.3906/yer-2011-18
- Mouthereau, F. 2011. Timing of uplift in the Zagros belt/ Iranian plateau and accommodation of late Cenozoic Arabia–Eurasia convergence. Geological Magazine, 148, 726–738, https://doi.org/10.1017/S00167568 11000306
- Murray, A. and Montgomery, D.W. 2014. Characterization of highly fractured basement, Say'un Masila Basin, Yemen. Geological Society, London, Special Publications, 374, 289–310, https://doi.org/10.1144/SP374.1
- Murris, R. 1980. Middle East: Stratigraphic evolution and oil habitat. *AAPG Bulletin*, **64**, 597–618.
- Ninkabou, D., Agard, P. et al. 2021. Structure of the offshore obducted Oman margin: emplacement of Semail ophiolite and role of tectonic inheritance. Journal of Geophysical Research: Solid Earth, 126, 2020JB020187, https://doi.org/10.1029/2020JB020 187
- Nonn, C., Leroy, S., Khanbari, K. and Ahmed, A. 2017. Tectono-sedimentary evolution of the eastern Gulf of Aden conjugate passive margins: narrowness and asymmetry in oblique rifting context. *Tectonophysics*, 721, 322–348, https://doi.org/10.1016/j.tecto.2017. 09 024
- Nonn, C., Leroy, S., Lescanne, M. and Castilla, R. 2019. Central Gulf of Aden conjugate margins (Yemen-Somalia): tectono-sedimentary and magmatism evolution in hybrid-type margins. *Marine and Petroleum Geology*, **105**, 100–123, https://doi.org/10.1016/j.marpetgeo.2018.11.053

- Noufal, A. and Obaid, K. 2016. Abu Dhabi Stress Map, UAE. SPE 182919–MS, Abu Dhabi International Petroleum Exhibition & Conference, 7–10 November 2016, Abu Dhabi, UAE.
- Perumalla, S., Al-Fares, A. *et al.* 2014. Regional in-situ stress mapping: an initiative for exploration & development of deep gas reservoirs in Kuwait. IPTC 2014: International Petroleum Technology Conference, January 2014, cp-395-00296.
- Pham, C., Chang, C., Jang, Y., Kutty, A. and Jeong, J. 2020. Effect of faults and rock physical properties on in situ stress within highly heterogeneous carbonate reservoirs. *Journal of Petroleum Science and Engineering*, 185, 106–601, https://doi.org/10.1016/j.petrol.2019. 106601
- Raba'a, A.S., Abbas, H., Hembling, D.E. and Finkbeiner, T. 2007. a geomechanical facies-based approach to optimize drilling and completion strategy of an unconsolidated sandstone reservoir, Saudi Arabia. SPE 109774, SPE Annual Technical Conference and Exhibition, 11–14 November 2007, Anaheim, California, USA.
- Rajabi, M., Tingay, M. and Heidbach, O. 2014. The present-day stress pattern in the Middle East and Northern Africa and their importance: The World Stress Map database contains the lowest wellbore information in these petroliferous areas. IPTC 2014: International Petroleum Technology Conference, January 2014, cp-395-00293.
- Reiter, K. and Heidbach, O. 2014. 3-D geomechanicalnumerical model of the contemporary crustal stress state in the Alberta Basin (Canada). Solid Earth, 5, 1123–1149, https://doi.org/10.5194/se-5-1123-2014
- Soroush, H., Gao, H., Qutob, H., Neil, B., Mahli, Z. and Abalioglu, I. 2011. Geomechanical study for UBD feasibility in the Northern Iraq Fields. SPE/IADE 146386, SPE/IADC Middle East Drilling Technology Conference and Exhibition, 24–26 October 2011, Muscat, Oman.
- Sperner, B., Müller, B., Heidbach, O., Delvaux, D., Reinecker, J. and Fuchs, K. 2003. Tectonic stress in the Earth's crust: advances in the World Stress Map project. *Geological Society, London, Special Publications*, 212, 101–116, https://doi.org/10.1144/GSL.SP.2003.212.
- Stern, R.J. and Johnson, P. 2010. Continental lithosphere of the Arabian Plate: a geologic, petrologic, and geophysical synthesis. *Earth-Science Reviews*, 101, 29–67, https://doi.org/10.1016/j.earscirev. 2010.01.002
- Tarapoanca, M., Andriessen, P. et al. 2010. Forward kinematic modelling of a regional transect in the Northern Emirates using geological and apatite fission track age constraints on paleo-burial history. Arabian Journal of Geosciences, 3, 395–411, https://doi.org/10.1007/s12517-010-0213-3
- Townend, J. and Zoback, M. 2004. Regional tectonic stress near the San Andreas fault in central and southern California. *Geophysical Research Letters*, 31, https://doi. org/10.1029/2003GL018918
- van-der-Zee, W., Ozan, C., Brudy, M. and Holland, M. 2011. 3D geomechanical modeling of complex salt structures. SIMULIA Customer Conference, 17–19 May 2011, Barcelona, Spain. 1–16.

- Viltres, R., Jónsson, S. et al. 2022. Present-day motion of the Arabian plate. Tectonics, 41, https://doi.org/10. 1029/2021TC007013
- Watremez, L., Leroy, S. *et al.* 2011. The crustal structure of the north-eastern Gulf of Aden continental margin: insights from wide-angle seismic data. *Geophysical Journal International*, **184**, 575–594, https://doi.org/10.1111/j.1365-246X.2010.04881.x
- Weidle, C., Wiesenberg, L., El-Sharkawy, A., Krüger, F., Scharf, A., Agard, P. and Meier, T. 2022. A 3-D crustal shear wave velocity model and Moho map below the Semail Ophiolite, eastern Arabia. *Geophysical Journal International*, 231, 817–834, https://doi.org/10.1093/ gji/ggac223
- Xu, W., Dutta, R. and Jonsson, S. 2015. Identifying active faults by improving earthquake locations with InSAR data and Bayesian estimation: the 2004 Tabuk (Saudi Arabia) Earthquake Sequence. Bulletin of the

- Seismological Society of America, 105, 765–775, https://doi.org/10.1785/0120140289
- Ziegler, M.A. 2001. Late Permian to Holocene paleofacies evolution of the Arabian plate and its hydrocarbon occurrences. *GeoArabia*, **6**, 445–504, https://doi.org/10.2113/geoarabia0603445
- Ziegler, M. and Heidbach, O. 2021. Manual of the Matlab Script FAST Calibration v2. 0. World Stress Map Technical Report 21-02, GFZ German Research Centre for Geosciences, https://doi.org/10.48440/wsm.2021. 002
- Ziegler, M.O., Heidbach, O., Reinecker, J., Przybycin, A.M. and Scheck-Wenderoth, M. 2016. A multi-stage 3-D stress field modelling approach exemplified in the Bavarian Molasse Basin. Solid Earth, 7, 1365–1382, https://doi.org/10.5194/se-7-1365-2016
- Zoback, M.D. 2010. *Reservoir Geomechanics*. Cambridge University Press, Cambridge.